

1 **SIM-HOM (version 1.0): a Mechanistic Module for the**
2 **formation of highly oxygenated organic molecules from**
3 **Isoprene, Monoterpene and Sesquiterpene evaluated with**
4 **ADCHAM (version 1.0)**

5
6 Liwen Yang¹, Wei Nie^{1, 2, *}, Mikael Ehn³, Chao Yan^{1, 2, 4}, Lubna Dada⁵, Yuliang Liu^{1, 2},
7 Pontus Roldin⁶ and Aijun Ding^{1, 2}

8
9 ¹ Joint International Research Laboratory of Atmospheric and Earth System Sciences,
10 School of Atmospheric Sciences, Nanjing University, Nanjing 210023, China

11 ² National Observation and Research Station for Atmospheric Processes and
12 Environmental Change in Yangtze River Delta, Nanjing 210023, China

13 ³ Institute for Atmospheric and Earth System Research/Physics, Faculty of Science,
14 University of Helsinki, Helsinki 00014, Finland

15 ⁴ Nanjing-Helsinki Institute in Atmospheric and Earth System Sciences, Nanjing
16 University, Nanjing 210023, China

17 ⁵ Laboratory of Atmospheric Chemistry, Paul Scherrer Institute, 5232 Villigen,
18 Switzerland

19 ⁶ Division of Combustion Physics, Department of Physics, Lund University, P. O. Box
20 118SE-221 00 Lund, Sweden

21 *Correspondence: Wei Nie (niewei@nju.edu.cn)

22

23 **Abstract**

24 Biogenic volatile organic compounds (BVOCs), including isoprene, monoterpenes, and
25 sesquiterpenes, are emitted in large quantities and play a critical role in atmospheric chemistry. They
26 contribute to the formation of highly oxygenated organic molecules (HOM), which are essential for
27 new particle formation (NPF) and secondary organic aerosol (SOA) formation. However, current
28 models often oversimplify the oxidation pathways of these compounds, leading to inaccuracies in
29 predicting HOM composition and concentrations. To address this gap, we developed a mechanistic
30 module, SIM-HOM (Sesquiterpene, Isoprene and Monoterpene-derived HOM mechanism), based
31 on Master Chemical Mechanism (MCM), that explicitly incorporates autoxidation processes,
32 detailed fragmentation pathways, and RO₂-RO₂ interactions for isoprene, monoterpene, and
33 sesquiterpenes. The updated module was validated using experimental data from the Cosmics
34 Leaving OUtdoor Droplets (CLOUD) chamber, demonstrating substantial improvements in
35 simulating HOM concentrations under various conditions. Specifically, it significantly improves the
36 simulation of highly oxidized isoprene products, resolves discrepancies in monoterpene-derived
37 HOM distributions, and provides the first comprehensive parameterization of sesquiterpene
38 oxidation products. The model also captures the HOM formation under mixed precursor conditions.
39 These advancements underscore the importance of incorporating detailed molecular-level reaction
40 mechanisms into atmospheric models. Future work should focus on refining branching ratios for
41 critical reactions and investigating the influence of temperature and nitrogen oxides on HOM
42 formation, and expanding the mechanism to include additional BVOC classes. Our findings provide
43 a robust foundation for improving global atmospheric simulations of SOA formation and climate
44 interactions.

45

46 **1.introduction**

47 The continental boundary layer is profoundly influenced by biogenic volatile organic compounds
48 (BVOC) emitted by vegetation. BVOC encompass diverse compounds, including isoprene, terpenes,
49 and related species, with specific types varying by vegetation type and environmental conditions.
50 The global annual emission flux of isoprene (C₅H₈) reaches up to 594 Tg, while monoterpenes
51 (C₁₀H₁₆) are emitted approximately 95 Tg annually, sustaining mixing ratio from parts per billion
52 (ppb) levels ppb to hundreds of parts per trillion (ppt). Collectively, isoprene and monoterpenes
53 contribute about 80% of total BVOC emissions (Sindelarova et al., 2014). Sesquiterpenes, such as
54 β-caryophyllene, are emitted around 20 Tg annually and are highly reactive compounds with a C15
55 skeleton. These BVOCs react rapidly with atmospheric oxidants, including hydroxyl radicals (OH),
56 ozone (O₃), and nitrate radicals (NO₃), producing low-volatility oxygenated vapors. Among these,
57 highly oxygenated organic molecules (HOM), are particular important as they significantly
58 contribute to particle nucleation (Kirkby et al., 2016; Riccobono et al., 2014; Lehtipalo et al., 2018),
59 growth (Simon et al., 2020; Stolzenburg et al., 2018; Trostl et al., 2016), and secondary organic
60 aerosol (SOA) formation (Ehn et al., 2014; Nie et al., 2022; Liu et al., 2023).

61 Peroxy radicals (RO₂) are critical intermediates in the atmospheric oxidation of BVOC and play a
62 central role in the formation of HOM. Under typical atmospheric conditions, a subset of RO₂ are
63 produced by the oxidation of monoterpenes and sesquiterpenes by O₃ or OH can undergo rapid
64 autoxidation during which internal H-shift and subsequent O₂ additions lead to the formation of

65 multifunctional, low-volatility compounds (Iyer et al., 2021; Berndt et al., 2016; Shen et al., 2022;
66 Richters et al., 2016b). The autoxidation rate is strongly sensitive to molecular structure, varying by
67 several orders of magnitude depending on functional groups, and shows significant positive
68 temperature dependence (Crouse et al., 2013; Praske et al., 2018; Moller et al., 2016; Jorgensen et
69 al., 2016; Knap and Jorgensen, 2017; Otkjaer et al., 2018). Concurrently, autoxidation competes
70 with bimolecular reactions involving NO_x , HO_2 , and other RO_2 . The RO_2 - HO_2 reaction typically
71 leads to the formation of hydroperoxides, which can contribute to HOM formation or undergo
72 further reaction. Additionally, RO_2 - RO_2 can result in the formation of HOM monomers, where two
73 RO_2 react to produce two new molecules, often with one less oxygen atom than their precursors.
74 RO_2 - RO_2 reactions can also form HOM dimers (Heinritzi et al., 2020; Berndt et al., 2018; Ng et al.,
75 2008), which are less volatile than HOM monomers and play a pivotal role in NPF and SOA
76 formation. The influence of nitrogen oxides (NO_x) on HOM formation is complex: NO exhibits a
77 nonlinear effect for cyclic monoterpenes, promoting HOM formation at low concentrations but
78 inhibiting it at higher levels (Nie et al., 2023); whereas for isoprene, HOM formation may increase
79 with NO (Berndt et al., 2025). NO_2 tends to suppress HOM formation by consuming acyl RO_2 .
80 Therefore, an accurate depiction of HOM formation requires consideration of autoxidation reactions
81 and its competition with bimolecular RO_2 reactions, which are influenced by atmospheric
82 composition, temperature, and the structure of the oxidizing molecules. Studies on the HOM
83 formation from isoprene are limited because of its smaller molecular weight (Shen et al., 2024; Zhao
84 et al., 2021; Wang et al., 2018; Xu et al., 2021; Curtius et al., 2024; Nie et al., 2022; Liu et al., 2021).
85 It can suppress HOM formation by scavenging large RO_2 radicals formed from the oxidation of
86 other VOCs (Heinritzi et al., 2020; Mcfiggans et al., 2019).

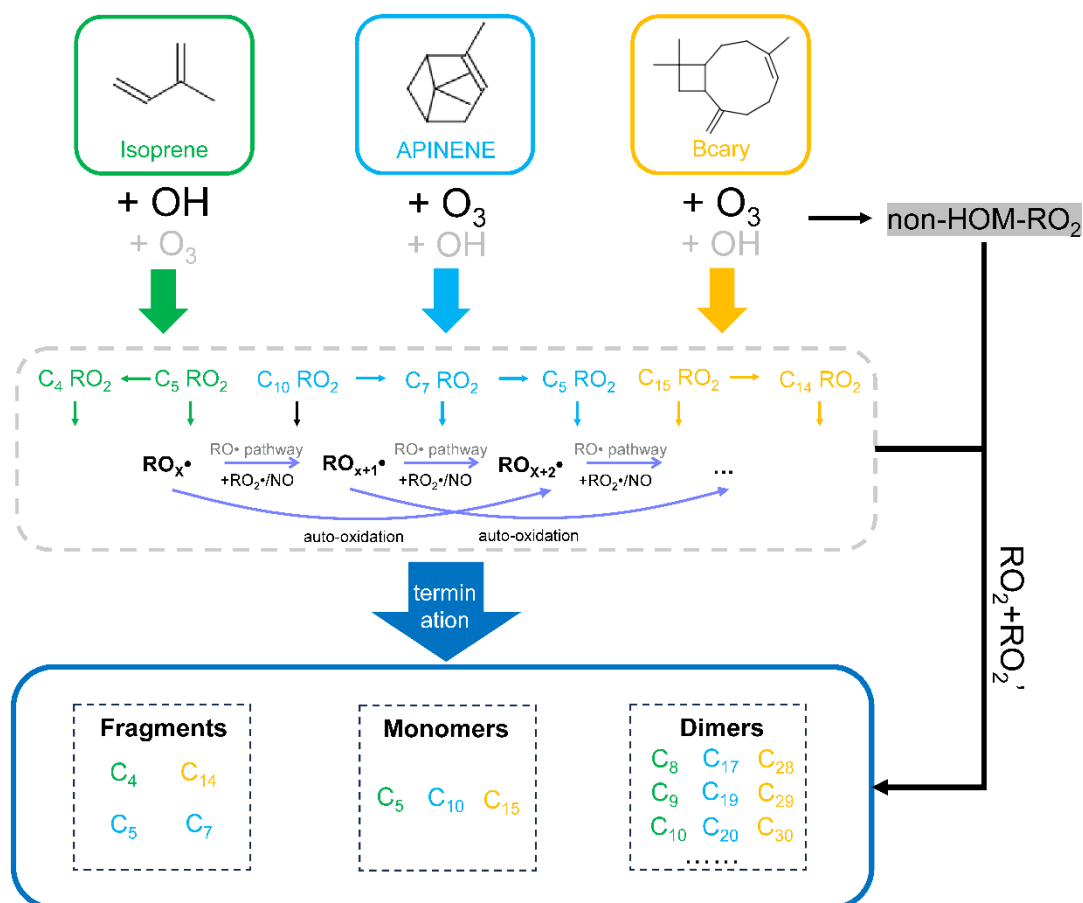
87 Insights into HOM formation mechanisms have highlighted the need to quantify their roles under
88 varying atmospheric conditions. This has been made possible by recent experimental advances, which
89 have driven the development of numerical models primarily targeting HOM mechanisms from
90 monoterpenes. Computationally efficient model like the radical two-dimensional Volatility Basic
91 Set (radical-VBS) by Schervish et al (Schervish and Donahue, 2020; Schervish et al., 2024) and
92 CRI-HOM (Weber et al., 2020) have been implemented in some large-scale models. These
93 frameworks are designed to represent the overall formation and partitioning behavior of HOM using
94 parameterized volatility distributions and oxidation pathways, rather than explicitly tracking
95 individual molecules. While grounded in mechanistic understanding, their simplified representation
96 may omit potential important aspects of chemical complexity, such as the role of specific RO_2
97 reaction pathways or the molecular identity of condensing vapors. Conversely, quasi-explicit
98 approaches, such as the method by Roldin et al (Roldin et al., 2019), provide detailed autoxidation
99 chemistry but lack comprehensive descriptions of fragmentation products. For isoprene oxidation
100 mechanisms, comprehensive models like the Master Chemical Mechanism (MCM) (Jenkin et al.,
101 2015) and Caltech isoprene mechanisms (Wennberg et al., 2018) incorporate detailed
102 representations of isoprene chemistry, consisting of hundreds of species (up to 602 in MCMv3.3.1
103 and 404 in the Caltech mechanism) and approximately 1000 reactions. While these existing models
104 emphasize radical budget, carbon cycling and SOA contributions, they often do not resolve the
105 specific HOM formation or accretion products in detail, due to their limited parameterizations.
106 Sesquiterpenes, though often omitted from current models, can exhibit HOM yields of around 2%
107 (Richters et al., 2016a; Jokinen et al., 2016) under laboratory conditions. Given their 15-carbon
108 structure, the resulting oxidation products are lower volatile than those from smaller VOCs,

109 allowing even modest HOM yields to contribute efficiently to particle-phase mass and new particle
110 growth.

111 Building upon these foundational studies, this study develops a unified and mechanistically detailed
112 mechanism, SIM-HOM (Sesquiterpene, Isoprene, and Monoterpene-derived HOM mechanism) that
113 extends HOM modeling to include not only monoterpenes and isoprene, but also sesquiterpenes, an
114 often overlooked yet potentially important contributor due to their low volatility oxidation products
115 (Dada et al., 2023). The model incorporates autoxidation and interactions among RO₂ radicals from
116 various VOCs, enabling a more comprehensive representation of HOM formation under
117 atmospherically relevant conditions. Section 2 details the model development based on existing gas-
118 phase chemical mechanisms and theoretical studies. Section 3 discusses the model validation using
119 the experiment data from Cosmics Leaving Outdoor Droplets (CLOUD) chamber, and section 4
120 summarizes this study and provides recommendations for future research.

121 **2. Mechanism development**

122 The mechanism developed in this study is primarily based on the MCM framework, chosen for its
123 comprehensive representation of organic compounds degradation in the troposphere and its ability
124 to incorporate a wide range of atmospheric chemical reactions with detailed kinetic and mechanistic
125 data. Within its framework, the gas-phase chemistry of isoprene was refined using updates from the
126 Caltech isoprene mechanism, focusing on the autoxidation pathway and HOM formation.
127 Monoterpene oxidation was addressed using modifications from the Peroxy Radical Autoxidation
128 Mechanism (PRAM), emphasizing fragmentations and ester formation as an accretion product. For
129 sesquiterpenes, a dedicated module was developed, leveraging both theoretical and experimental
130 data to represent its distinctive chemical pathways to HOM formation. Additionally, we
131 incorporated detailed interactions between different RO₂ species, including dimer formation. Figure
132 1 illustrates the primary framework of this mechanism, with specific attention to the roles of
133 unimolecular and bimolecular reactions in driving HOM production. Detailed modifications to the
134 base mechanism are described in the following sections.



135

136 Figure 1. Schematic plot showing the mechanism of HOM formation via the oxidation of isoprene,
 137 monoterpenes and sesquiterpenes in the absence of NO_x. Isoprene is primarily oxidized by OH,
 138 while monoterpenes and sesquiterpenes are primarily oxidized by O₃. A small fraction of RO₂ can
 139 undergo autoxidation (defined as p-HOM-RO₂, colored font in the figure), and the other fraction of
 140 RO₂ that cannot undergo autoxidation (defined as non-HOM-RO₂, grey-bottomed font in the figure).
 141 p-HOM-RO₂ can undergo both unimolecular and bimolecular reactions, and both can form alkoxy
 142 radicals, which can fragment or isomerize. For the dimer formation, we only consider them from
 143 RO₂-RO₂ reactions between p-HOM-RO₂ and non-HOM-RO₂.

144

145 2.1 Extension of Isoprene Oxidation Mechanism

146 In recent decades, significant advancements have been made in understanding the oxidation
 147 mechanisms of isoprene, due to its key role in atmospheric chemistry and its extremely high
 148 abundance in the atmosphere. As the most emitted BVOC globally, isoprene has been widely
 149 recognized as a significant SOA precursor, forming specific intermediates such as isoprene-
 150 epoxydiol (IEPOX) (Paulot et al., 2009; Nguyen et al., 2014) and methacryloyl peroxyoxynitrate
 151 (MPAN) (Nguyen et al., 2015), in addition to highly functionalized low-volatility compounds
 152 (Krechmer et al., 2015; D'arnbro et al., 2017; Xu et al., 2021).

153 Accurately representing the isoprene chemistry in large-scale atmospheric models is crucial but
 154 remains challenging due to the complex reaction mechanisms. MCM, through continuous updates,
 155 provides an almost complete compilation of isoprene's degradation pathways. Additionally,

156 Wennberg et al. (2018) conducted a systematic review of current knowledge on isoprene chemistry,
157 resulting in the development of the Caltech isoprene mechanism—a detailed reaction framework
158 capable of dynamically simulating the allylic and peroxy radical systems formed when isoprene
159 reacts with OH radicals (Wennberg et al., 2018). Compared to earlier mechanisms, the Caltech
160 isoprene mechanism introduces significant advancements, including the incorporation of reversible
161 O₂ addition to allyl radicals, the identification of new products from 1,6-H shifts in Z-δ-OH-peroxy
162 radicals, and a reduced yield of C₅-hydroperoxy-aldehydes (HPALD). Furthermore, it includes more
163 intramolecular H-shift processes, such as rapid peroxy-hydroperoxyl (RO₂-OOH) shifts, which
164 enhance OH recycling rates under low-nitrogen conditions. Despite these advancements, MCM
165 provides a more detailed treatment of isoprene chemistry, including more comprehensive RO₂-RO₂
166 reactions and improved photolysis processes. The photolysis rate constants in MCM are calculated
167 by integrating light flux over specific wavelengths, enabling accurate representation of photolysis
168 under varying atmospheric conditions. In contrast, the Caltech mechanism calculates photolysis
169 rates using a simplified coefficient, 'sun', which relies on sunrise and sunset times. While effective
170 for outdoor scenarios, this approach does not adequately capture the intricacies of controlled
171 laboratory illumination, making MCM the preferred mechanism for laboratory-based simulations.

172 To exploit the strengths of both mechanisms, we integrated the MCM and Caltech isoprene
173 mechanisms in our framework. This posed significant challenges due to differences in species
174 naming conventions between the two frameworks. In the MCM, compounds are named
175 systematically based on their chemical structure and assigned a unique identifier, whereas the
176 Caltech mechanism employs a naming system based on the carbon skeleton and functional group
177 positions. As a result, careful mapping of chemical species between the two mechanisms was
178 required to bridge these discrepancies (see Supplementary Information for details). This integrated
179 approach allows us to harness the complementary advantages of both mechanisms for a more robust
180 representation of isoprene chemistry.

181 Despite these improvements, the descriptions of HOM production from the oxidation of isoprene
182 remain incomplete. To address this gap, we incorporated autoxidation pathways for specific high-
183 yield RO₂ formed during isoprene oxidation, which are crucial intermediates in isoprene oxidation.
184 The key RO₂ radicals considered include those substituted with =O, -OH, and -OOH groups, which
185 originate from isoprene hydroxyperoxyl radicals (ISOPOO) and RO₂ species formed following a
186 1,6 α-hydroxy H-shift in two Z-δ-ISOPOO isomers. The rapid H-shift reactions of these high-yield
187 RO₂ radicals are critical, as they allow for the production of stable, low-volatility products under
188 typical atmospheric conditions, making them particularly potent for HOM formation.

189 For these H-shift reactions to compete effectively with bimolecular reactions involving NO, HO₂,
190 and other RO₂, unimolecular reaction rate constants need to reach approximately $\sim 10^{-2} \text{ s}^{-1}$ or higher.
191 Reported H-shift rates for these radicals cover a wide range, from 8.2×10^{-2} to $3.0 \times 10^5 \text{ s}^{-1}$ at 298
192 K (Moller et al., 2019), with hydroperoxides exhibiting notably faster rate. While the Caltech
193 isoprene mechanism assumes alkyl radicals predominantly fragment into smaller products, thus
194 limiting HOM formation, we introduced an oxygen addition pathway to alkyl radicals, as suggested
195 in (Wang et al., 2018). This modification introduces a competing reaction pathway that can produce
196 new RO₂ species, counterbalancing the dominance of fragmentation. Subsequent bimolecular
197 reactions involving these RO₂ species were implemented based on the work of (Jenkin et al., 2019).

198 Although OH oxidation overwhelmingly dominates the removal of isoprene from the atmosphere,

199 O_3 oxidation accounts for approximately 10% of isoprene's global loss (Bates and Jacob, 2019).
200 Previous models primarily focused on its contributions to the formation of methyl vinyl ketone
201 (MVK), methacrolein (MACR), CH_2OO (C1 SCI), and OH, while largely neglecting its potential
202 contribution to HOM formation. Here, we adopted a simplified approach similar to that of
203 (Schervish et al., 2024), assuming that only a small fraction of RO_2 radicals are capable of
204 undergoing autoxidation. These RO_2 radicals can subsequently participate in unimolecular or
205 bimolecular reactions, with some contributing to the HOM formation.

206 **2.2 Improvement of Monoterpene Oxidation Mechanism**

207 Our model extends the first comprehensive Peroxy Radical Autoxidation Mechanism (PRAM)
208 developed by (Roldin et al., 2019). PRAM meticulously simulates the autoxidation processes of
209 RO_2 formed from monoterpene oxidation. This mechanism has demonstrated strong agreement with
210 observed HOM concentrations, SOA mass concentrations, and NPF in boreal forest simulations.
211 However, the original PRAM only considered the HOM formation pathway via monoterpene
212 oxidation by O_3 and OH. Nie et al later expanded this mechanism by incorporating NO_3 -initiated
213 oxidation pathway to the original mechanism, which mainly includes the autoxidation of
214 monoterpenes by NO_3 to form RO_2 ; the reaction of RO_2 with NO_3 to form RO radicals (though this
215 pathway is negligible under most environmental conditions) and bimolecular termination reactions
216 between NO_2 and specific RO_2 (e.g., acyl RO_2). (Nie et al., 2023)

217 In this study, we further optimize the key oxidation pathways of monoterpenes, with a particular
218 focus on α -pinene ozonolysis, which serves as a representative case due to its atmospheric relevance
219 and detailed mechanistic understanding. Conventional mechanisms propose that α -pinene
220 ozonolysis begins with the decomposition of the primary ozonide into a carbonyl-substituted
221 Criegee Intermediate (CI). Three isomeric forms of this CI can undergo a 1,4 H-shift to produce
222 vinyl hydroperoxide (VHP). The VHP subsequently decomposes into a vinyloxy radical, which reacts
223 with O_2 to form a RO_2 radical. However, under typical conditions, the isomerization of this RO_2
224 radical is too slow to explain the observed rapid formation of HOMs. To address this, (Iyer et al.,
225 2021) proposed a critical solution by introducing a chemically activated ring-opening reaction of
226 one of the vinyloxy radicals. This reaction leads to the rapid formation of an endoperoxide and a RO_2
227 radical with a high oxygen content (containing 8 oxygen atoms). The PRAM mechanism
228 incorporates this modification and further details the progressive increase in oxygen atoms within
229 the molecule through consecutive intramolecular RO_2 H-shifts and O_2 additions during autoxidation.
230 This autoxidation chain ultimately terminates through bimolecular reactions with NO, HO_2 , or other
231 RO_2 radicals, forming a variety of products such as alkoxy radicals, closed-shell HOM monomers,
232 or dimers. Once alkoxy radicals are formed, they may undergo further transformations. For example,
233 they can isomerize into hydroxy-substituted alkyl radicals, which subsequently react with O_2 to
234 form new RO_2 species, or they may form closed-shell HOM monomers with additional carbonyl
235 groups. Alternatively, they may decompose into more volatile species. A specific example of these
236 fragment products includes the MCM-modeled RO_2 species C717O2 (an RO_2), and smaller volatile
237 species like acetone (CH_3COCH_3).

238 In our improved model, we incorporated the C7-fragment due to recent studies indicate that early-
239 formed addition products retain sufficient energy to overcome transition state barriers, leading to
240 the formation of a significant amount of alkyl radicals with an endoperoxide group (EPO). Unlike
241 the traditional view that excess energy dissipates in the next O_2 addition step, (Yang et al., 2025)

242 demonstrated that EPO formation enables rearrangement pathways involving alkoxy radicals with
243 epoxide groups (AOE). Their study identified that cleavage reactions from these intermediates,
244 which yield acetone and C₇ products (AE-C7), are the fastest. Furthermore, the O₂ addition products
245 (RO₂) formed from AE-C7 and AE-C10 contain multiple active sites for H-shift, facilitating further
246 autoxidation. These findings provide key insights into the competition between unimolecular H-
247 shift reactions and bimolecular sinks, such as reactions with NO and HO₂. Additionally, the
248 contribution of AE-C7 and AE-C10 derivatives explains observed peaks in mass spectrometry
249 corresponding to C₇-HOMs.

250 We also incorporated RO₂-Kb β-cleavage and CH₂O loss to better represent the formation of C₁₉
251 accretion products, like C₁₉H₂₈O_x and C₁₉H₃₀O_x, as observed in experiments by Berndt et al. (Berndt
252 et al., 2018). These products are formed through RO₂ self- and cross-reactions involving CH₂O loss.
253 Furthermore, experiments that isolated OH oxidation revealed that these C₁₉ accretion products are
254 not formed through pure OH-mediated processes, but rather arise specifically from O₃-derived RO₂
255 radicals (Peräkylä et al., 2023; Kenseth et al., 2023). Our updated model explicitly accounts for
256 these distinctions, differentiating the contributions of OH- versus O₃-derived RO₂ radicals in the
257 formation of HOM accretion products.

258 **2.3 Development of Sesquiterpene Oxidation Mechanism**

259 Prior to our work, HOM formation from sesquiterpenes lacked a dedicated module in atmospheric
260 models. To address this, we developed a comprehensive framework based on the reaction pathways
261 proposed by (Richters et al., 2016b), integrating key processes derived from existing knowledge to
262 better represent the oxidation chemistry of sesquiterpenes. Given that β-caryophyllene is the only
263 sesquiterpene included in MCM, our development focuses exclusively on this compound.

264 The ozonolysis of β-caryophyllene begins with an exothermic reaction between O₃ and the double
265 bonds of sesquiterpene molecules, forming CIs with significant excess energy. These chemically
266 activated CIs can either stabilize through collisions with other molecules or undergo unimolecular
267 reactions. Stable CIs may also engage in bimolecular reactions, initiating a variety of pathways that
268 eventually lead to HOM formation. A critical step involves the isomerization of CIs into vinyl
269 hydroperoxide, which further decomposes by releasing OH radicals, producing alkyl radicals as
270 intermediates. The alkyl radicals rapidly react with O₂, forming the first generation of RO₂ radical.

271 The fate of these initial RO₂ radicals branch into several pathways. In one major pathway, the RO₂
272 radical undergoes intramolecular H-shifts followed by O₂ addition, resulting in new RO₂ radicals
273 that resemble the first-generation p-HOM-RO₂ species observed in monoterpene ozonolysis. These
274 products typically include hydroperoxide (-OOH) functionalities. Alternatively, RO₂ radicals can
275 attack the remaining double bond in the sesquiterpene structure. This process leads to the formation
276 of endoperoxides and additional alkyl radicals, which subsequently react with O₂ to form new RO₂
277 radicals, though these lack the -OOH functional group. Further reaction pathways are also possible.
278 For instance, RO₂ radicals may undergo additional intramolecular H-shifts, resulting in the
279 formation of closed-shell products along with the release of OH radicals; or the subsequent O₂
280 addition after H-shift forms a new RO₂. Another pathway involves internal RO₂ reactions with the
281 remaining double bond, which can generate cyclic R radicals. These cyclic radicals then react with
282 O₂, producing the next generation of RO₂ radicals.

283 Epoxide formation is another potential pathway, where an epoxide ring forms within the molecule,

284 followed by cleavage of the acyl alkoxy functionality and the expulsion of CO₂. This step yields
285 alkyl radicals that rapidly react with O₂ to form new RO₂ species. These RO₂ radicals can then enter
286 further autoxidation processes, involving a series of intramolecular hydrogen transfer reactions and
287 successive O₂ additions, to produce higher-generation RO₂ species.

288 By systematically integrating these reaction pathways into our model, we developed a robust
289 framework to simulate HOM formation from sesquiterpene ozonolysis. The inclusion of detailed
290 autoxidation chemistry, along with pathways involving both -OOH and non-OOH functional group
291 formation, ensures a more comprehensive representation of the sesquiterpene oxidation process and
292 its contribution to atmospheric HOM and SOA formation.

293 **2.4 RO₂ cross reactions in mixed VOC system**

294 In real atmospheric conditions, VOC mixtures produce a variety of RO₂ radicals that can react with
295 each other to form RO, closed-shell monomers, or dimers. Given the vast number of RO₂ species in
296 detailed chemical mechanisms, explicitly representing all possible cross-reactions is impractical. To
297 address this, MCM uses a simplified approach, which assumes that all RO₂ radicals interact
298 uniformly within a "RO₂ pool" at a collective rate. This is implemented using the parameter $\Sigma[\text{RO}_2]$,
299 which represents the summed concentration of all RO₂ species. Within this framework, the total rate
300 of all possible cross-reactions for a particular RO₂ radical is approximated as a pseudo-unimolecular
301 reaction with a rate coefficient of $k \times \Sigma[\text{RO}_2]$. While this simplification reduces computational
302 complexity, it overlooks the specific contributions of individual RO₂ combinations, particularly in
303 processes like dimer formation. The CRI-HOM model addresses dimerization by treating it as a
304 simplified reaction in which one RO₂ radical produces half of the total dimer product. Although
305 efficient, this approach fails to account for differences in how specific RO₂ combinations influence
306 product distributions.

307 In our improved model, we redefine dimerization as a specific bimolecular reaction between distinct
308 RO₂ species. To reduce complexity, we focus on the interactions between two key types of RO₂:
309 those capable of autoxidation and those that cannot undergo autoxidation (as represented in MCM).
310 Autoxidizable RO₂ radicals, due to their higher degree of functionalization, exhibit faster
311 dimerization rates (Berndt et al., 2018). Non-autoxidizable RO₂ radicals, which are generally
312 present at higher concentrations, can serve as reaction partners in these bimolecular reactions.
313 Reactions between two autoxidizable RO₂ are not explicitly represented, due to their extremely low
314 concentrations, which makes their contribution to dimer formation negligible. Likewise, reactions
315 between two non-autoxidizable RO₂ are not treated as explicit accretion product formation pathways
316 due to due to their products are probably not HOM. Instead, these reactions remain represented
317 within the generic RO₂ loss framework of the RO₂ pool, where they contribute to closed-shell
318 monomer formation through the pseudo-unimolecular reaction scheme. In this way, the total RO₂-
319 RO₂ reaction flux among all RO₂ species is still accounted for, while only those combinations most
320 relevant for HOM dimer formation are treated explicitly.

321 RO₂ + RO₂ rate coefficients are assigned according to the overall oxidation state and molecular size
322 of the RO₂ radicals, using the number of oxygen atoms as a proxy for the degree of functionalization.
323 This approach is consistent with the parameterization described above, where more highly
324 oxygenated and generally larger RO₂ radicals are assumed to exhibit higher reactivity in RO₂ + RO₂
325 reactions. SIM-HOM uses RO₂ + RO₂ reaction rates leading to closed-shell monomer products in

326 the range of 1×10^{-12} to 1.5×10^{-11} cm^3s^{-1} and $\text{RO}_2 + \text{RO}_2$ reactions leading to HOM dimers in the
327 range of 1×10^{-14} to 1.5×10^{-12} cm^3s^{-1} . This choice reflects the generally smaller branching fraction of
328 the accretion channel relative to the formation of monomer products. As a result, the effective
329 branching ratio toward accretion products in the model is typically on the order of $\sim 10\%$, consistent
330 with recent experimental and theoretical studies (Murphy et al., 2025; Berndt et al., 2018). Because
331 these dimers arise from explicit bimolecular reactions, the identities of these products are
332 determined by the specific pair of reacting RO_2 precursors. This approach balances computational
333 efficiency with improved accuracy, capturing the variability in RO_2 reactions and their impact on
334 product distributions, particularly in mixed VOC systems.

335 **2.5 Summary of the Model Improvements**

336 We implemented several key updates to the model, focusing on the autoxidation pathway, RO_2 - RO_2
337 interaction, fragmentation and termination processes. Together, these enhancements provide a more
338 accurate and comprehensive representation of atmospheric oxidation, enabling better simulation of
339 VOC oxidation and HOM formation:

340 (1) Expanded Autoxidation Pathways

341 We refined the autoxidation scheme for isoprene, monoterpenes, and sesquiterpenes by
342 incorporating recent experimental and theoretical advancements. Key updates include 1) High-yield
343 RO_2 autoxidation reactions for isoprene oxidation; 2) Extended formation and autoxidation
344 pathways for C_7 - RO_2 species in monoterpene oxidation; 3) Integration of new autoxidation and
345 HOM formation processes for sesquiterpenes, building on the MCM framework.

346 (2) Improved RO_2 - RO_2 Interactions

347 For permutation reactions, we maintained MCM's computationally efficient method. However, for
348 dimer formation, we moved beyond the simplified treatments used in mechanisms like CRI-HOM.
349 Our model explicitly parameterizes RO_2 - RO_2 interactions based on their VOC origins and
350 incorporates β -cleavage reactions for RO_2 from monoterpene ozonolysis during dimerization. This
351 provides a more detailed representation of dimer distributions and the behavior of mixed VOC
352 systems.

353 (3) Updated Fragmentation and Termination Pathways

354 We incorporated detailed fragmentation mechanisms for monoterpene and sesquiterpene oxidation
355 products, enabling more accurate predictions of experimental product distributions. Additionally,
356 new pathways for alkoxy radical formation and subsequent secondary RO_2 radicals were introduced,
357 improving the representation of carbon distribution among the oxidized products.

358 **3. Model Validation Based on CLOUD Experiments**

359 We validated the constructed model using experimental data from the Cosmic Leave Outdoor
360 Droplet Chamber (CLOUD) at CERN. The experiments were conducted in a 26.1 cm^3 stainless steel
361 chamber that can simulate diverse atmospheric conditions under well-controlled environments.
362 Specifically, we utilized data from the CLOUD 11 campaign conducted in the fall of 2016 (Dada et
363 al., 2023; Heinritzi et al., 2020). These experiments included oxidation of single precursors (pure
364 isoprene, α -pinene, and β -caryophyllene) and their mixtures, such as α -pinene and isoprene, or α -
365 pinene, isoprene, and β -caryophyllene. Table 1 summarizes the experimental conditions. For the
366 mixed experiments, the precursor molar ratio (sesquiterpene: monoterpene: isoprene) was set to

367 1:6:50 to mimic typical BVOC emissions in the atmosphere. Most pure α -pinene and β -
 368 caryophyllene experiments were performed under dark conditions, with OH concentration of
 369 approximately $1 \times 10^6 \text{ cm}^{-3}$, formed primarily via the BVOCs reactions with O_3 . When isoprene was
 370 added, OH is predominantly consumed by isoprene, resulting in a further lower OH concentration.
 371 To increase OH concentrations, Hamamatsu UV lamps (UVH) and UV excimer lasers (UVX) were
 372 employed. No NO_x was introduced in the experiments, effectively excluding NO_3 oxidation
 373 pathways. The CLOUD chamber is one of the most advanced reactors for replicating atmospheric
 374 conditions, ensuring that the lifetime and reaction pathways of p-HOM-RO₂ in the chamber closely
 375 resemble those in the real atmosphere. This allows p-HOM-RO₂ to undergo sufficient autoxidation.
 376 The oxidation products, i.e., oxygenated organic molecules, were measured using a nitrate chemical
 377 ionization atmospheric pressure interface time-of-flight (CI-API-ToF) mass spectrometer.

378

379 Table 1. Summary of the experimental conditions used in this study. All experiments are performed
 380 at 5°C and 40% RH.

	Exp	isoprene (ppt)	α -pinene (ppt)	Bcary (ppt)	O_3 (ppb)	UVH	UVX
isoprene system	IP-4500	4456	0	0	37.5	off	off
	IP-4500	4214	0	0	41.5	off	on
monoterpene system	MT-300	0	340	0	40.7	off	off
	MT-600	0	666	0	40.2	off	off
	MT-1200	0	1165	0	39.3	off	off
	MT-1200	0	1059	0	39.7	off	on
Sesquiterpene system	SQT-1.8	0	0	1.8	47.8	off	off
	SQT-3.3	0	0	3.3	48.5	off	off
	SQT-6.6	0	0	6.6	47.6	off	off
	SQT-6.6	0	0	6.6	48.7	on	off
Mixed system I: isoprene and monoterpene	Mix I-MT300	3962	317	0	44.9	off	off
	Mix I-MT600	3780	618	0	46.4	off	off
	Mix I-MT1200	3588	1116	0	47.6	off	off
	Mix I-MT1200	3396	1096	0	47.9	on	on
Mixed system II: isoprene, monoterpene and sesquiterpene	Mix II-Low	1471	303	3	45.6	on	off
	Mix II-Medium	2695	578	7.1	45.7	on	off
	Mix II-High	5749	1168	15.8	44.3	on	off
	Mix II-High	4578	974	15.8	44.3	on	on

381

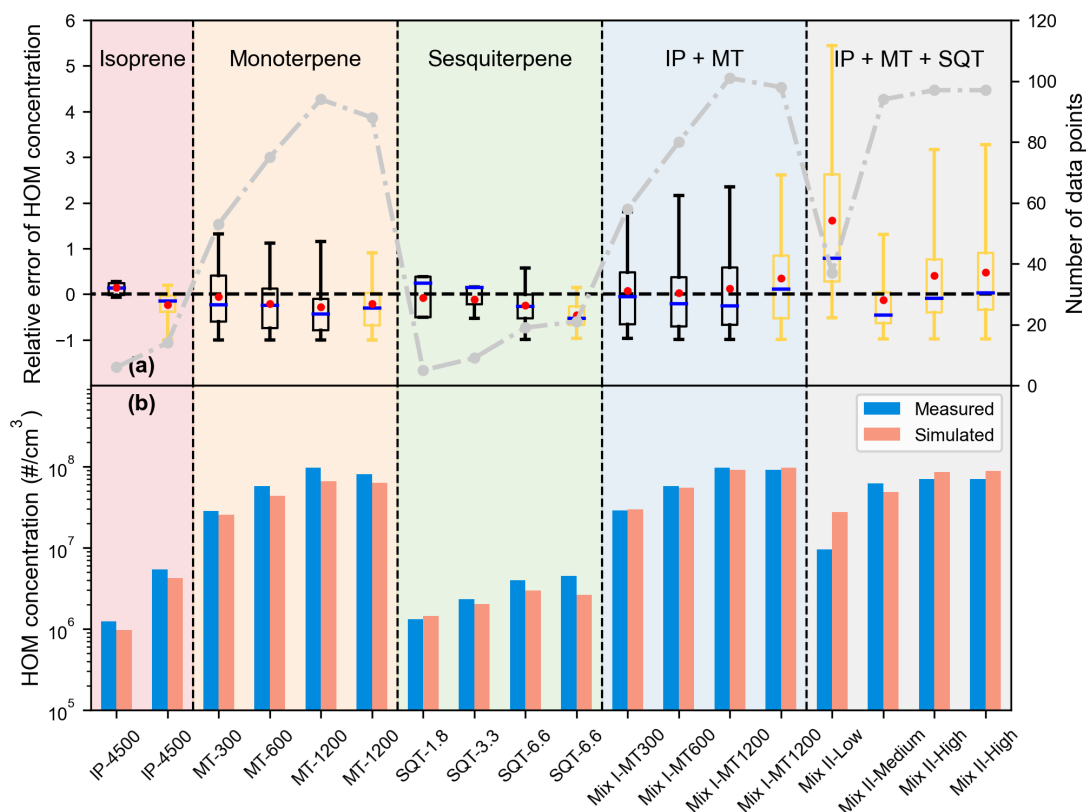
382 Our initial chemical mechanism did not account for deposition or condensation onto pre-existing
 383 aerosol surfaces. To address this limitation and isolate the effects of gas-phase chemistry, we
 384 coupled the chemical mechanism with the Aerosol Dynamics, gas- and particle-phase chemistry
 385 model for laboratory CHAMber studies (ADCHAM) (Roldin et al., 2014). ADCHAM integrates
 386 modules for aerosol dynamics, particle-phase chemistry, and a kinetic multilayer model to account

387 for diffusion-limited transport between the gas phase, particle surface, and particle bulk. Once the
388 chamber reactions reached steady-state, we simulated the HOM concentrations and compared the
389 results with experimental data. By iteratively adjusting the rate constants for autoxidation and
390 accretion product formation, we refined the chemical mechanism to achieve the best agreement with
391 experimental observations.

392 **3.1 Overall comparison**

393 To assess the model's performance under varying environmental conditions, we calculated the
394 relative error of HOM concentrations by normalizing the difference between observed and simulated
395 concentrations. Only species with concentrations exceeding $5 \times 10^4 \text{ cm}^{-3}$ (the CI-APi-ToF detection
396 limit) were considered. As shown in Figure 2a, the relative errors (defined as the difference between
397 modeled and measured HOM concentrations normalized by the measurements) are illustrated as
398 box plots. They remain close to 0 under most conditions, indicating strong agreement between
399 model and measurements. However, in the mixed system of three VOCs (IP + MT + SQT),
400 particularly at low VOC concentrations, larger discrepancies appear. This may be attributed to
401 photolysis of oxidation products by UVH lamps, which is not explicitly considered in detail, leading
402 to deviations in HOM predictions. The number of selected data points (gray dashed line) also varies
403 across different conditions, influencing error estimates.

404 Figure 2b compares the simulated and observed HOM concentrations across different VOC systems.
405 The total HOM concentration varies significantly across different precursors. The isoprene system
406 produces relatively lower HOM concentrations compared to monoterpene and sesquiterpene
407 systems, consistent with the expected differences in oxidation pathways and HOM formation
408 efficiency. The monoterpene system exhibits the highest HOM concentrations, particularly at higher
409 precursor concentrations, followed by the sesquiterpene system. In mixed systems, including the
410 isoprene-monoterpene system (Mix I) and the three-VOC mixture (Mix II), the total HOM
411 concentration increases compared to the isoprene-only system, reflecting the contribution of
412 monoterpenes and sesquiterpenes. The model successfully reproduces the general trends, capturing
413 the HOM concentrations in isoprene, monoterpene, and sesquiterpene systems, as well as in mixed
414 systems. However, overestimation is observed in some cases, particularly in low VOC concentration
415 scenarios, as discussed earlier, likely due to incomplete representation of photolysis processes.
416 Despite these minor deviations, the overall variations in HOM production across different VOC
417 regimes are well reproduced.



418

419 Figure 2. (a) Boxplots of relative errors and (b) comparison of simulated HOM and observations
 420 under different experimental conditions. From left to right, they represent pure isoprene,
 421 monoterpene, and sesquiterpene systems, the mixed system of isoprene, monoterpene, and
 422 the mixed system of the three VOCs. The specific experimental conditions are shown in Table 1.
 423 Boxplots represent medians, quartiles, and 5-95% percentiles, with red circles indicating the median,
 424 where the boxes are black in dark conditions and yellow in light conditions. The grey line indicates
 425 the number of HOM with higher concentration than the detection limit under each experimental
 426 condition. Blue and outer circles indicate observed values, pink and inner circles indicate simulated
 427 values.

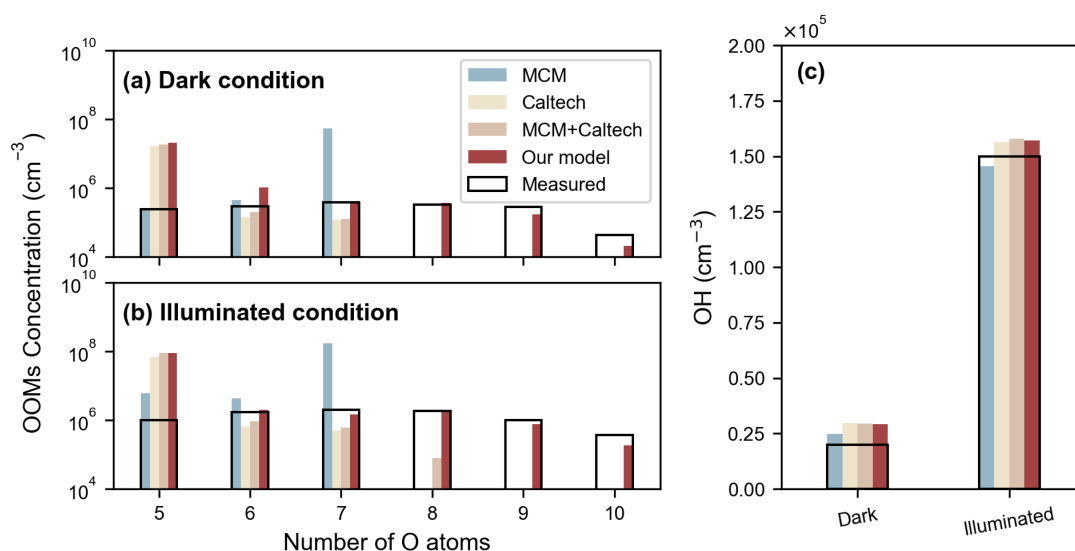
428

429 3.1 Isoprene system

430 In the pure isoprene system, the isoprene was continuously injected to maintain a concentration
 431 between 4 and 5 ppb, while O₃ was approximately 40 ppb, under both dark and illuminated
 432 conditions. We compared the simulation results from our improved module, MCM, the Caltech
 433 isoprene mechanism (Caltech), and their combination (MCM + Caltech). All models showed strong
 434 performance in predicting OH concentration (Fig. 3c).

435 Across different experimental conditions, our model exhibits significant advantages in capturing the
 436 distribution of highly oxygenated oxidation products compared to other models. For OOMs
 437 containing 5 oxygen atoms, all four models predicted concentrations notably higher than the
 438 experimental measurements (Fig. 3a and 3b), likely due to the reduced sensitivity of the NO₃⁻ CI-
 439 APi-ToF mass spectrometer towards OOMs with five or fewer oxygen atoms (Riva et al., 2019).
 440 For OOMs with six or seven oxygen atoms, the MCM model significantly overestimated their

441 concentrations, while the Caltech model underestimated them. In contrast, our model closely
 442 matched the measured data, indicating superior accuracy in simulating these oxidized species. More
 443 importantly, for OOMs containing eight or more oxygen atoms, our model was the only one capable
 444 of capturing their formation, underscoring its ability to accurately represent the complex pathways
 445 of HOM formation during isoprene oxidation.



446

447 Figure 3. Comparison of measured and simulated results from four models (our improved model,
 448 MCM, Caltech, and MCM + Caltech): (a) oxidation products with varying numbers of oxygen atoms
 449 under dark conditions, (b) oxidation products under illuminated conditions, and (c) OH
 450 concentration under both dark and illuminated conditions.

451 Recent studies have demonstrated that isoprene-derived highly oxygenated organic molecules (IP-
 452 HOMs) play a key role in new particle formation (NPF) in the upper troposphere (Curtius et al.,
 453 2024; Shen et al., 2024; Zha et al., 2024). Our model effectively simulates the formation of HOMs,
 454 underscoring its relevance for investigating the mechanisms of NPF and subsequent particle growth.
 455 However, the observed HOM spectrum in our chamber experiments differs from that of the
 456 atmosphere due to weak OH recycling, a consequence of the absence of NO_x and the predominantly
 457 dark or low-light experimental conditions. Atmospheric OH· levels during daytime typically remain
 458 above 10⁶ cm⁻³, even in the presence of isoprene, sustaining secondary oxidation processes. As a
 459 result, atmospheric isoprene oxidation predominantly produces C₅H₁₂O_x, C₅H₁₁NO_x and C₅H₁₀N₂O_x
 460 via second-generation OH oxidation from ISOPOOH and isoprene hydroxy nitrate (Curtius et al.,
 461 2024; Shen et al., 2024; Zha et al., 2024; Xu et al., 2021). In contrast, our experimental spectrum is
 462 dominated by C₅H₈₋₁₀O_x (Fig.S2), derived from the mono- and bimolecular reaction of RO₂ formed
 463 directly via isoprene oxidation. A comparison of C₅H₁₂O_x concentrations with other C₅ compounds
 464 (Fig.S3) further confirms that second-generation oxidation plays a minimal role in our experiments.
 465 Despite these differences, our model integrates all relevant oxidation pathways, providing a more
 466 comprehensive representation of isoprene oxidation chemistry.

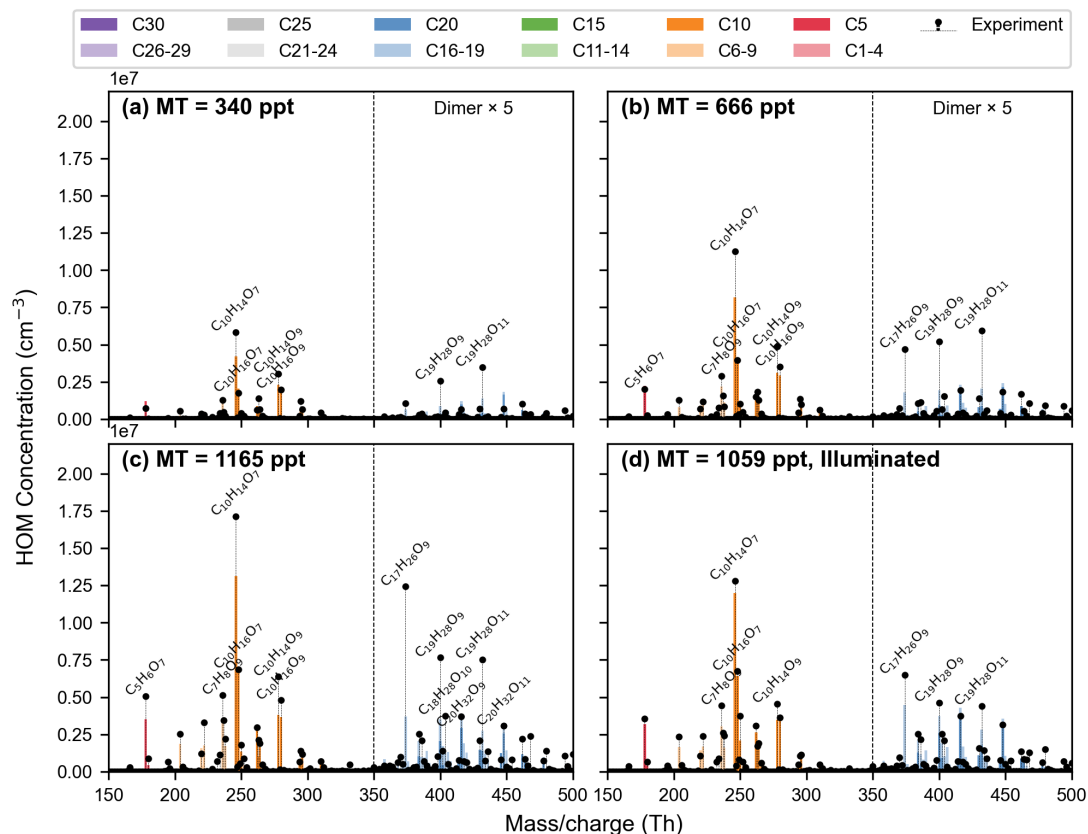
467

468 3.2 Monoterpene system

469 Fig. 4 presents the predicted oxidation products spectrum from our improved model alongside

470 experimental measurement under different conditions. A detailed comparison with the experimental
471 data demonstrates that our model achieves high accuracy in reproducing monoterpene oxidation
472 processes. In particular, it effectively captures the formation of RO₂ radicals with 10 carbon atoms
473 (C₁₀-RO₂) and accurately simulates their subsequent reaction pathways. Fragment simulation has
474 traditionally been a challenge in numerical modeling. In our improved model, we incorporated C₇
475 fragments formation by incorporating recent findings on early-stage product cleavage (Yang et al.,
476 2025). The model successfully reproduces the isomerization of C₁₀-RO₂, leading to carbon skeleton
477 cleavage and C₇-RO₂ formation, which undergoes autoxidation and termination to produce C₇-
478 HOMs. Furthermore, C₇-RO₂ produces C₅-RO₂ through RO pathway, accurately simulating key
479 fragment products such as C₅H₆O₇, validating the model's capability in capturing essential oxidation
480 pathways.

481 Beyond accurately representing the main monomer and fragmentation product distributions, the
482 model also exhibits significant improvements in simulating dimer formation. In particular, the
483 enhanced formation of C₇-RO₂ has led to an improved prediction of C₁₇H₂₆O₉ concentration, which
484 corresponds to the most abundant dimer observed in our measurements. Additionally, the
485 incorporation of RO₂-Kb β-cleavage and CH₂O loss processes have contributed to the relatively
486 high concentrations of C₁₉H₂₈O₉ and C₁₉H₂₈O₁₁ dimers. Despite these advancements, the model still
487 slightly underestimates these dimer concentrations compared to experimental observations. Several
488 factors may contribute to this discrepancy. First, the actual yield of RO₂-Kb is higher than estimated
489 in MCM (Meder et al., 2025), leading to an underrepresentation of key dimer-forming precursors.
490 Second, RO₂-Kb cleavage products may have a higher efficiency in forming accretion products
491 compared to other RO₂, an aspect not fully accounted for in the current model. Third, additional
492 RO₂ species beyond those currently considered may undergo similar cleavage reactions,
493 contributing to dimer formation through pathways not yet incorporated (Peräkylä et al., 2023).
494 Addressing these uncertainties by refining the branching ratios and reaction rate constants of
495 dimerization pathways could help resolve these discrepancies and further improve the model's
496 predictive capabilities.



497

498 Figure 4. Comparisons between modeled and observed spectrum in α -pinene oxidation experiment
 499 with (a) 340 ppt, (b) 666 ppt, (c) 1165 ppt and (d) 1059 ppt α -pinene in (a-c) dark condition and (d)
 500 UV excimer laser (UVX) on. Mass/charge ratio is plotted in units of thomsons (Th) and it should be
 501 noted that the nitrate reagent ions has been removed from mass.

502

503 3.3 Sesquiterpene system

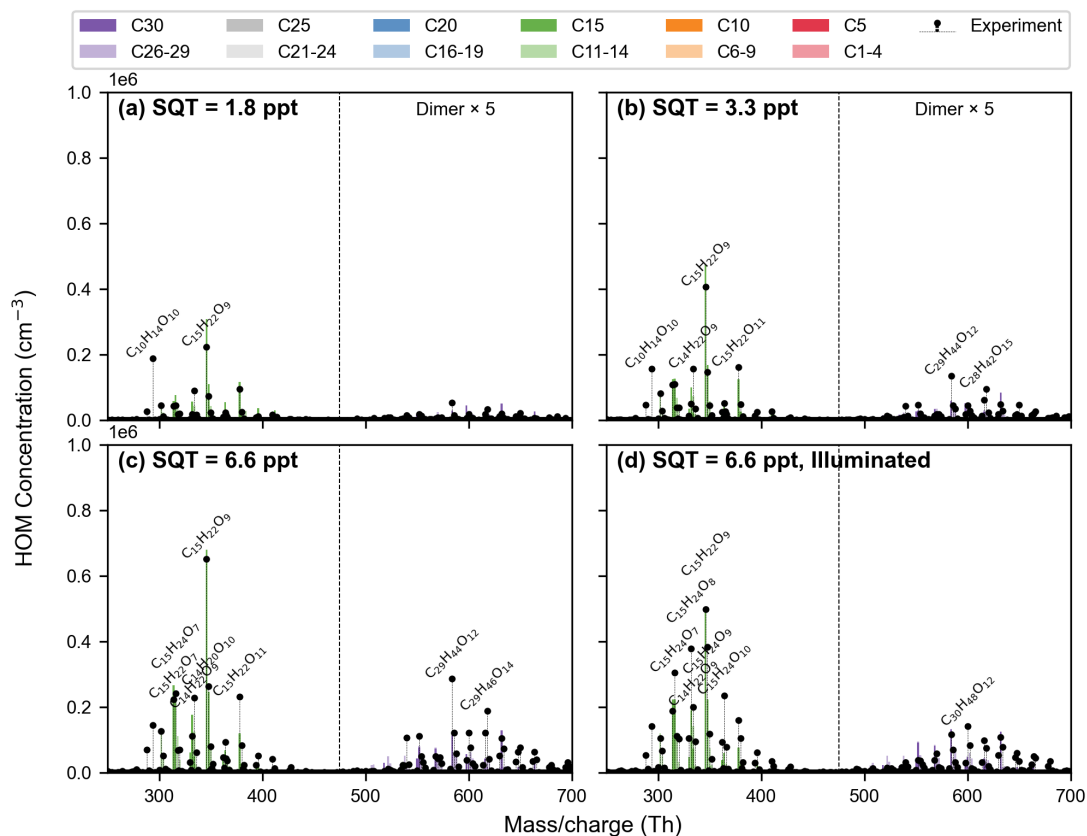
504 Fig. 5 shows that our newly developed sesquiterpene-HOM model is in strong agreement with the
 505 experimental data. During the validation process, we meticulously compared the model predictions
 506 with experimental results obtained under controlled conditions, ensuring that key chemical products
 507 - including fragmentation products, monomers, and dimers - were accurately represented. The
 508 model accurately captures the formation and transformation of these products, confirming its
 509 reliability in simulating sesquiterpene oxidation.

510 A key achievement of the model is its accurate prediction of $C_{15}H_{22}O_9$, the most abundant HOM
 511 molecule under these experimental conditions and a critical ELVOC contributing to NPF (Dada et
 512 al., 2023). This highlights the model's ability to capture the dominant oxidation pathways of
 513 sesquiterpenes. To comprehensively describe the reaction mechanism, we incorporated an epoxide
 514 formation step, in which CO_2 is expelled from the acyl alkoxy functional group of the intermediate,
 515 forming an alkyl radical that rapidly reacts with O_2 to form an RO_2 radical. This modification
 516 successfully explains the observed C_{14} fragmentation product, further improving the model's
 517 accuracy in reproducing experimental spectrum. However, while the model successfully reproduces
 518 the observed peaks for most monomers and fragments, it fails to predict $C_{10}H_{14}O_{10}$, which is

519 detected at non-negligible concentrations in experiments. This discrepancy arises from the absence
 520 of reported formation pathways for this compound, suggesting that additional reaction mechanisms
 521 may need to be explored.

522 Regarding dimer formation, the model incorporates detailed RO₂ cross-reaction pathways. While
 523 the model provides a reasonable overall prediction, it overestimates the concentrations of lower-
 524 molecular-mass dimers while underestimating the most abundant dimers, such as C₂₉H₄₄O₁₂ and
 525 C₂₉H₄₆O₁₄. This suggests that refinements in the reaction rates governing dimerization processes-
 526 particular the relative contribution of RO₂-RO₂ from fragment RO₂ are necessary to achieve better
 527 agreement with observations. Additionally, the inclusion of alternative dimerization channels, such
 528 as those involving secondary oxidation, may be required to better represent the observed dimer
 529 distribution.

530 Overall, the strong agreement between model predictions and experimental data indicates that our
 531 model effectively captures the fundamental oxidation mechanism governing sesquiterpene-derived
 532 HOM formation. By incorporating detailed reaction pathways and refining key parameters, the
 533 model not only reproduces observed concentration but also provides mechanistic insights into HOM
 534 formation. These advancements establish our sesquiterpene-HOM module as a valuable tool for
 535 simulating complex chemistry under atmospheric conditions.

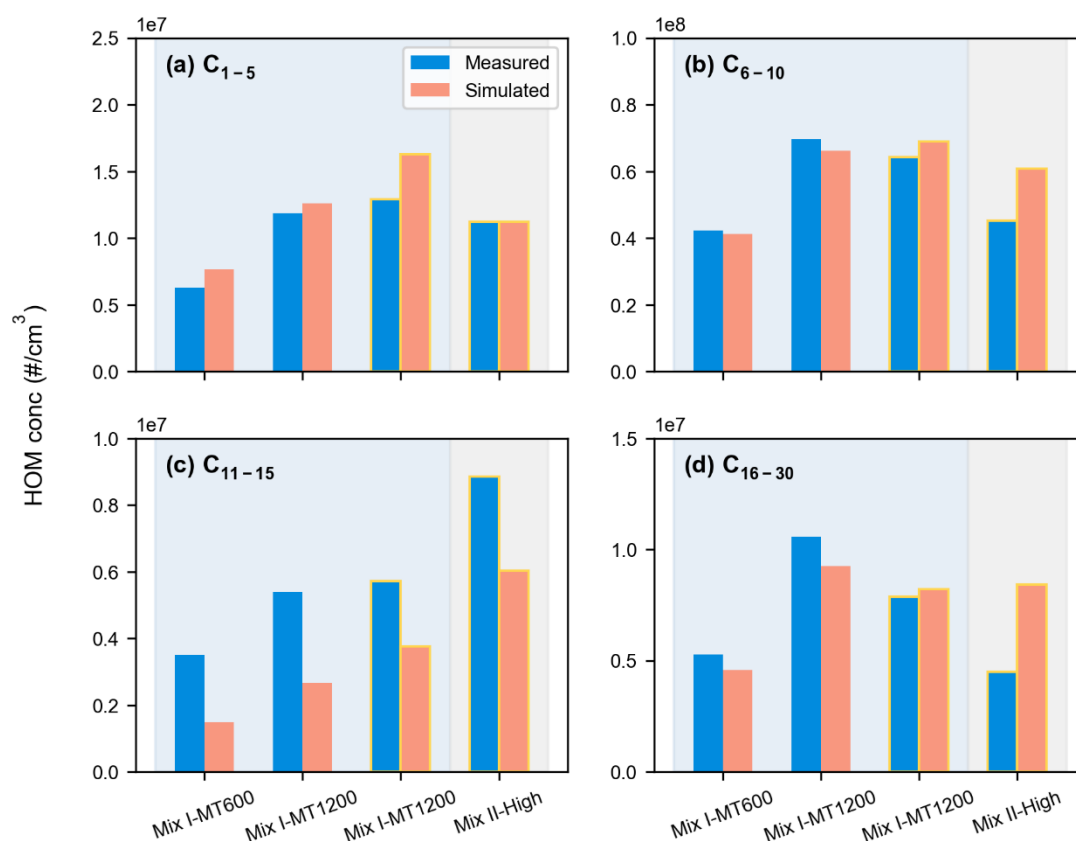


536

537 Figure 5. Comparisons between modeled and observed spectrum in β -caryophyllene oxidation
 538 experiment with (a) 1.8 ppt, (b) 3.3 ppt and (c-d) 6.6 ppt β -caryophyllene in (a-c) dark condition
 539 and (d) Hamamatsu UV lamps (UVH) on. Mass/charge ratio is plotted in units of thomsons (Th)
 540 and it should be noted that the nitrate reagent ions has been removed from mass.

541 3.4 Mixed system

542 In this section, we compared the observed and simulated HOM concentrations in mixed systems
 543 under various conditions, including different VOC combinations, changes in VOC concentrations
 544 and the introduction of UV light (see Fig.S4 and Fig.S5). Across all cases, the simulations overall
 545 matched the observed HOM distributions, accurately reproducing key peaks and maintaining the
 546 expected carbon number distributions. Additionally, we analyzed the variation in HOM
 547 concentrations with different carbon numbers for four representative mixing conditions: (1) a
 548 mixture of isoprene and monoterpenes (Mix I-MT600), (2) an increased monoterpene concentration
 549 (Mix I-MT1200), (3) the introduction of UV light (Mix I-MT1200, Illuminated), and (4) the
 550 subsequent addition of sesquiterpenes (Mix II-High, Illuminated).



551

552 Figure 6. Experimental and simulated HOM concentration for different carbon numbers in four
 553 different mix systems (Mix I-MT600: 600 ppt α -pinene + 4 ppb isoprene; Mix I-MT1200: 1200
 554 ppt α -pinene + 4 ppb isoprene; Mix I-MT1200: 1200 ppt α -pinene + 4 ppb isoprene, illuminated;
 555 Mix II-High: 1200 ppt α -pinene + 6 ppb isoprene + 16 ppt β -caryophyllene, illuminated,
 556 respectively.). Blue bars indicate observed values and pink bars indicate simulated values, where no
 557 edge color indicates dark conditions and yellow edge color indicates light conditions. The light blue
 558 background indicates the mixed system I of isoprene and monoterpenes, and the grey background
 559 indicates the mixed system II of the three VOCs. The specific experimental conditions are shown in
 560 Table 1.

561

562 In the initial isoprene–monoterpene mixture, oxidation led to a diverse range of HOMs from both

563 C₅- and C₁₀-RO₂ pathways (Fig. S4a). Increasing the monoterpene concentration enhanced HOM
564 formation, particularly for monoterpene-derived species, like C₆₋₁₀- and C₁₆₋₂₀-HOMs (from Mix I-
565 MT600 to Mix I-MT1200, Fig.6b and 6d). The introduction of UV light shifted the HOM
566 distribution by promoting isoprene oxidation, leading to an increase in C₁₋₅- and C₁₁₋₁₅-HOMs (from
567 Mix I-MT1200 to Mix I-MT1200, illuminated, Fig.6a and 6c) while reducing monoterpene-derived
568 termination products, in particular dimers with more than 15 carbon atoms. However, the model
569 underestimated C₁₁₋₁₅-HOM concentrations, likely due to an underrepresentation of cross-reaction
570 between isoprene-derived and monoterpene-derived RO₂. The addition of sesquiterpenes further
571 altered HOM distribution, notably increasing C₁₁₋₁₅-HOM (Fig.6c), suggesting sesquiterpenes
572 exhibit a higher propensity for autoxidation and further amplifying these product channels. However,
573 the significant decrease in C₁₆₋₃₀-HOM concentration observed in three-VOC mixture, which was
574 not reflected in the simulations (Fig.6d), could be attributed to the overestimated rate of dimer
575 formation involving sesquiterpenes. This shift was likely driven by the competitive consumption of
576 available RO₂ radicals, which are reflected in both observations and models. Our model's ability to
577 simulate key features—such as the redistribution of HOM classes due to competitive RO₂
578 chemistry—demonstrates its robustness in simulating the oxidation of complex VOC mixtures. This
579 agreement highlights the model's capability to provide mechanistic insights into HOM formation
580 under varied atmospheric conditions.

581 **4. Conclusion**

582 In this study, we developed a novel and comprehensive mechanism, SIM-HOM (Sesquiterpene,
583 Isoprene, and Monoterpene-derived HOM mechanism), for simulating the HOM formation from
584 isoprene, monoterpenes, and sesquiterpenes. This mechanism incorporates intricate processes such
585 as autoxidation and interactions among RO₂ radicals derived from various BVOC, providing a more
586 nuanced understanding of the chemical transformations leading to HOM formation. The mechanism
587 was rigorously optimized and validated using experimental data obtained from the CLOUD chamber,
588 thereby demonstrating its robust capability to accurately reproduce the observed concentrations of
589 HOMs under various conditions. From an atmospheric perspective, this model is particularly
590 valuable for understanding NPF and SOA formation. Recent studies have highlighted the nucleating
591 potential of isoprene-derived HOMs, a process that our mechanism captures effectively. In fact, our
592 model is the only one capable of simulating isoprene HOMs, which represents a crucial
593 advancement in understanding NPF. Another key innovation of our work is the refinement of the
594 monoterpene oxidation mechanism, which was already recognized as crucial in previous models,
595 but is now further optimized to improve its representation of HOM formation. Furthermore, the
596 inclusion of sesquiterpene-derived HOMs, which are key contributors to NPF as shown in recent
597 literature, makes this model the first to integrate these VOCs-derived HOM in a comprehensive
598 framework. Importantly, the improved HOM parameterization introduced here bridges the gap
599 between detailed gas-phase chemistry and aerosol-phase processes. It is increasingly recognized
600 that not all HOM contribute equally to SOA formation: some exhibit low volatility and can
601 irreversibly condense onto particles, while others are semi-volatile and may evaporate on short
602 timescales. Our framework captures these differences by resolving HOM at a near-molecular level,
603 thereby improving predictions of both short-lived SOA and more stable aerosol mass that influences
604 air quality and climate-relevant properties, such as cloud formation. Overall, our model significantly
605 enhances the ability of atmospheric simulations to link specific oxidation pathways to aerosol
606 formation outcomes, thereby offering a more mechanistic foundation for understanding and

607 predicting NPF and SOA formation across diverse environments.

608 However, several limitations need to be addressed. First, the model does not yet fully incorporate
609 NO_x-related pathways. Given the significant role of NO_x in HOM formation, especially in polluted
610 environments, refining these pathways is critical for improving predictions under high-NO_x
611 conditions. In particular, the potential contribution of NO₃-initiated oxidation to HOM formation is
612 not yet represented in the current version of the model. Recent studies suggest that the importance
613 of NO₃ chemistry is strongly compound-dependent. For example, laboratory measurements indicate
614 that HOM yields from isoprene + NO₃ reactions (~1.2%) (Zhao et al., 2021) are substantially higher
615 than those from isoprene oxidation by O₃ or OH (Jokinen et al., 2015), implying that NO₃ chemistry
616 may represent an important nighttime source of HOMs from isoprene. For larger BVOCs such as
617 sesquiterpenes, their multiple double bonds and high reactivity may also favor rapid autoxidation
618 following NO₃ addition, potentially leading to efficient HOM formation. In contrast, monoterpenes
619 already exhibit substantial HOM production through O₃ and OH oxidation (Ehn et al., 2014; Kirkby
620 et al., 2016), suggesting that NO₃ chemistry may play a less dominant role, although it could still
621 contribute under certain nocturnal conditions. Due to the limited availability of systematic
622 experimental data, particularly for isoprene and sesquiterpene NO₃ oxidation, these pathways are
623 not yet explicitly included in the present mechanism and represent an important direction for future
624 model development.

625 Additionally, the model does not yet incorporate photolysis reactions comprehensively, which can
626 significantly alter the fate of HOMs and oxidation products under experimental conditions, such as
627 utilizing UV lamps in the CLOUD chamber. Moreover, in the isoprene mechanism,
628 multigenerational oxidation plays a crucial role, but its contribution to HOMs in laboratory
629 experiments is likely lower than observed in the atmosphere. Another limitation lies in the branching
630 ratios of key reactions, which govern the probability of different chemical pathways during
631 autoxidation. Refining these ratios will be essential for the model's predictive capability. Expanding
632 the mechanism to include a wider range of VOCs and their oxidation products, and considering the
633 influence of environmental factors like temperature and atmospheric composition, will further
634 improve its applicability under diverse conditions.

635 Looking forward, an important challenge lies in simplifying the mechanism for integration into
636 computationally efficient atmospheric models, such as global or regional climate models. While our
637 mechanism provides valuable insights into the chemical processes of HOM formation, its
638 complexity poses a challenge for large-scale simulations. Developing simplified parameterizations
639 that retain the key atmospheric processes while reducing computational costs will be a key step in
640 facilitating its integration into broader atmospheric models for climate and air quality forecasting.
641 In conclusion, this model represents a significant advancement in understanding of HOM formation
642 and its role in atmospheric processes. However, further improvements, especially in refining NO_x
643 interactions, photolysis processes and constraining multigenerational oxidation in the isoprene
644 system, are necessary to fully realize its potential. And efforts to simplify the mechanism for large-
645 scale models, will be essential for broader implementation in atmospheric science and policy.

646

647 **Code and data availability.**

648 The ADCHAM (version 1.0) code coupled with SIM-HOM (version 1.0) mechanism used in this

649 study is publicly available at <https://doi.org/10.5281/zenodo.19047874> (Yang et al., 2026). The
650 repository also includes the model output generated in this study.

651

652 **Author contributions.**

653 W.N. designed the study. L.Y performed model simulations and analyzed the data. W.N., M.E, C.Y.,
654 L.D, Y.L., P.R. and A.D. are acknowledged for valuable discussions. L.Y. and W.N wrote the
655 manuscript. M.E. and L.D. contributed to editing the manuscript.

656

657 **Competing interests.**

658 The authors declare that they have no conflict of interest.

659

660 **Acknowledgements.**

661 We thank CERN-CLOUD for providing experimental data. This work was supported by the
662 National Natural Science Foundation of China (NSFC) project (42220104006), the Jiangsu Province
663 Outstanding Youth Fund (BK20240067), the Natural Science Foundation of Jiangsu Province
664 (BK20230773), the Jiangsu Provincial Collaborative Innovation Center of Climate Change, and the
665 Fundamental Research Funds for the Central Universities.

666

667 **Reference:**

668 Bates, K. H. and Jacob, D. J.: A new model mechanism for atmospheric oxidation of isoprene: global
669 effects on oxidants, nitrogen oxides, organic products, and secondary organic aerosol, *Atmos. Chem.*
670 *Phys.*, 19, 9613-9640, 10.5194/acp-19-9613-2019, 2019.

671 Berndt, T., Hoffmann, E. H., Tilgner, A., and Herrmann, H.: Highly oxidized products from the
672 atmospheric reaction of hydroxyl radicals with isoprene, *Nat. Commun.*, 16, 12, 10.1038/s41467-025-
673 57336-1, 2025.

674 Berndt, T., Mender, B., Scholz, W., Fischer, L., Herrmann, H., Kulmala, M., and Hansel, A.: Accretion
675 Product Formation from Ozonolysis and OH Radical Reaction of α -Pinene: Mechanistic Insight and the
676 Influence of Isoprene and Ethylene, *Environ. Sci. Technol.*, 52, 11069-11077, 10.1021/acs.est.8b02210,
677 2018.

678 Berndt, T., Richters, S., Jokinen, T., Hyttinen, N., Kurten, T., Otkjaer, R. V., Kjaergaard, H. G., Stratmann,
679 F., Herrmann, H., Sipila, M., Kulmala, M., and Ehn, M.: Hydroxyl radical-induced formation of highly
680 oxidized organic compounds, *Nat. Commun.*, 7, 10.1038/ncomms13677, 2016.

681 Crouse, J. D., Nielsen, L. B., Jorgensen, S., Kjaergaard, H. G., and Wennberg, P. O.: Autoxidation of
682 Organic Compounds in the Atmosphere, *J. Phys. Chem. Lett.*, 4, 3513-3520, 10.1021/jz4019207, 2013.

683 Curtius, J., Heinritzi, M., Beck, L. J., Pöhlker, M. L., Tripathi, N., Krumm, B. E., Holzbeck, P.,
684 Nussbaumer, C. M., Pardo, L. H., Klimach, T., Barmounis, K., Andersen, S. T., Bardakov, R., Bohn, B.,
685 Cecchini, M. A., Chaboureau, J. P., Dauhut, T., Dienhart, D., Dörich, R., Edtbauer, A., Giez, A., Hartmann,
686 A., Holanda, B. A., Joppe, P., Kaiser, K., Keber, T., Klebach, H., Krüger, O. O., Kürten, A., Mallaun, C.,
687 Marno, D., Martinez, M., Monteiro, C., Nelson, C., Ort, L., Raj, S. S., Richter, S., Ringsdorf, A., Rocha,
688 F., Simon, M., Sreekumar, S., Tsokankunku, A., Unfer, G. R., Valenti, I. D., Wang, N. J., Zahn, A.,
689 Zauner-Wieczorek, M., Albrecht, R. I., Andreae, M. O., Artaxo, P., Crowley, J. N., Fischer, H., Harder,
690 H., Herdies, D. L., Machado, L. A. T., Pöhlker, C., Pöschl, U., Possner, A., Pozzer, A., Schneider, J.,

691 Williams, J., and Lelieveld, J.: Isoprene nitrates drive new particle formation in Amazon's upper
692 troposphere, *Nature*, 636, 23, 10.1038/s41586-024-08192-4, 2024.

693 D'Arnbro, E. L., Moller, K. H., Lopez-Hilfiker, F. D., Schobesberger, S., Liu, J. M., Shilling, J. E., Lee,
694 B., Kjaergaard, H. G., and Thornton, J. A.: Isomerization of Second-Generation Isoprene Peroxy Radicals:
695 Epoxide Formation and Implications for Secondary Organic Aerosol Yields, *Environ. Sci. Technol.*, 51,
696 4978-4987, 10.1021/acs.est.7b00460, 2017.

697 Dada, L., Stolzenburg, D., Simon, M., Fischer, L., Heinritzi, M., Wang, M. Y., Xiao, M., Vogel, A. L.,
698 Ahonen, L., Amorim, A., Baalbaki, R., Baccarini, A., Baltensperger, U., Bianchi, F., Daellenbach, K. R.,
699 DeVivo, J., Dias, A., Dommen, J., Duplissy, J., Finkenzeller, H., Hansel, A., He, X. C., Hofbauer, V.,
700 Hoyle, C. R., Kangasluoma, J., Kim, C., Kürten, A., Kvashnin, A., Mauldin, R., Makhmutov, V., Marten,
701 R., Mentler, B., Nie, W., Petäjä, T., Quéléver, L. L. J., Saathoff, H., Tauber, C., Tome, A., Molteni, U.,
702 Volkamer, R., Wagner, R., Wagner, A. C., Wimmer, D., Winkler, P. M., Yan, C., Zha, Q. Z., Rissanen, M.,
703 Gordon, H., Curtius, J., Worsnop, D. R., Lehtipalo, K., Donahue, N. M., Kirkby, J., El Haddad, I., and
704 Kulmala, M.: Role of sesquiterpenes in biogenic new particle formation, *Science Advances*, 9,
705 10.1126/sciadv.adi5297, 2023.

706 Ehn, M., Thornton, J. A., Kleist, E., Sipila, M., Junninen, H., Pullinen, I., Springer, M., Rubach, F.,
707 Tillmann, R., Lee, B., Lopez-Hilfiker, F., Andres, S., Acir, I. H., Rissanen, M., Jokinen, T., Schobesberger,
708 S., Kangasluoma, J., Kontkanen, J., Nieminen, T., Kurten, T., Nielsen, L. B., Jorgensen, S., Kjaergaard,
709 H. G., Canagaratna, M., Dal Maso, M., Berndt, T., Petaja, T., Wahner, A., Kerminen, V. M., Kulmala, M.,
710 Worsnop, D. R., Wildt, J., and Mentel, T. F.: A large source of low-volatility secondary organic aerosol,
711 *Nature*, 506, 476-479, 10.1038/nature13032, 2014.

712 Heinritzi, M., Dada, L., Simon, M., Stolzenburg, D., Wagner, A. C., Fischer, L., Ahonen, L. R.,
713 Amanatidis, S., Baalbaki, R., Baccarini, A., Bauer, P. S., Baumgartner, B., Bianchi, F., Brilke, S., Chen,
714 D. X., Chiu, R., Dias, A., Dommen, J., Duplissy, J., Finkenzeller, H., Frege, C., Fuchs, C., Garmash, O.,
715 Gordon, H., Granzin, M., El Haddad, I., He, X. C., Helm, J., Hofbauer, V., Hoyle, C. R., Kangasluoma,
716 J., Keber, T., Kim, C., Kürten, A., Lamkaddam, H., Laurila, T. M., Lampilahti, J., Lee, C. P., Lehtipalo,
717 K., Leiminger, M., Mai, H. J., Makhmutov, V., Manninen, H. E., Marten, R., Mathot, S., Mauldin, R. L.,
718 Mentler, B., Molteni, U., Müller, T., Nie, W., Nieminen, T., Onnela, A., Partoll, E., Passananti, M., Petäjä,
719 T., Pfeifer, J., Pospisilova, V., Quéléver, L. L. J., Rissanen, M. P., Rose, C., Schobesberger, S., Scholz,
720 W., Scholze, K., Sipilä, M., Steiner, G., Stozhkov, Y., Tauber, C., Tham, Y. J., Vazquez-Pufleau, M.,
721 Virtanen, A., Vogel, A. L., Volkamer, R., Wagner, R., Wang, M. Y., Weitz, L., Wimmer, D., Xiao, M., Yan,
722 C., Ye, P. L., Zha, Q. Z., Zhou, X. Q., Amorim, A., Baltensperger, U., Hansel, A., Kulmala, M., Tomé,
723 A., Winkler, P. M., Worsnop, D. R., Donahue, N. M., Kirkby, J., and Curtius, J.: Molecular understanding
724 of the suppression of new-particle formation by isoprene, *Atmospheric Chemistry and Physics*, 20,
725 11809-11821, 10.5194/acp-20-11809-2020, 2020.

726 Iyer, S., Rissanen, M. P., Valiev, R., Barua, S., Krechmer, J. E., Thornton, J., Ehn, M., and Kurtén, T.:
727 Molecular mechanism for rapid autoxidation in α -pinene ozonolysis, *Nat. Commun.*, 12, 6,
728 10.1038/s41467-021-21172-w, 2021.

729 Jenkin, M. E., Young, J. C., and Rickard, A. R.: The MCM v3.3.1 degradation scheme for isoprene,
730 *Atmospheric Chemistry and Physics*, 15, 11433-11459, 10.5194/acp-15-11433-2015, 2015.

731 Jenkin, M. E., Valorso, R., Aumont, B., and Rickard, A. R.: Estimation of rate coefficients and branching
732 ratios for reactions of organic peroxy radicals for use in automated mechanism construction, *Atmospheric
733 Chemistry and Physics*, 19, 7691-7717, 10.5194/acp-19-7691-2019, 2019.

734 Jokinen, T., Kausiala, O., Garmash, O., Peräkylä, O., Junninen, H., Schobesberger, S., Yan, C., Sipilä,

735 M., and Rissanen, M. P.: Production of highly oxidized organic compounds from ozonolysis of β -
736 caryophyllene: laboratory and field measurements, *Boreal Environment Research*, 21, 262-273, 2016.

737 Jokinen, T., Berndt, T., Makkonen, R., Kerminen, V. M., Junninen, H., Paasonen, P., Stratmann, F.,
738 Herrmann, H., Guenther, A. B., Worsnop, D. R., Kulmala, M., Ehn, M., and Sipilä, M.: Production of
739 extremely low volatile organic compounds from biogenic emissions: Measured yields and atmospheric
740 implications, *Proc. Natl. Acad. Sci. U. S. A.*, 112, 7123-7128, 10.1073/pnas.1423977112, 2015.

741 Jorgensen, S., Knap, H. C., Otkjaer, R. V., Jensen, A. M., Kjeldsen, M. L. H., Wennberg, P. O., and
742 Kjaergaard, H. G.: Rapid Hydrogen Shift Scrambling in Hydroperoxy-Substituted Organic Peroxy
743 Radicals, *J. Phys. Chem. A*, 120, 266-275, 10.1021/acs.jpca.5b06768, 2016.

744 [Kenseth, C. M., Hafeman, N. J., Rezugui, S. P., Chen, J., Huang, Y. L., Dalleska, N. F., Kjaergaard, H. G.,
745 Stoltz, B. M., Seinfeld, J. H., and Wennberg, P. O.: Particle-phase accretion forms dimer esters in pinene
746 secondary organic aerosol, *Science*, 382, 787-792, 10.1126/science.adi0857, 2023.](#)

747 Kirkby, J., Duplissy, J., Sengupta, K., Frege, C., Gordon, H., Williamson, C., Heinritzi, M., Simon, M.,
748 Yan, C., Almeida, J., Trostl, J., Nieminen, T., Ortega, I. K., Wagner, R., Adamov, A., Amorim, A.,
749 Bernhammer, A. K., Bianchi, F., Breitenlechner, M., Brilke, S., Chen, X. M., Craven, J., Dias, A., Ehrhart,
750 S., Flagan, R. C., Franchin, A., Fuchs, C., Guida, R., Hakala, J., Hoyle, C. R., Jokinen, T., Junninen, H.,
751 Kangasluoma, J., Kim, J., Krapf, M., Kurten, A., Laaksonen, A., Lehtipalo, K., Makhmutov, V., Mathot,
752 S., Molteni, U., Onnela, A., Perakyla, O., Piel, F., Petaja, T., Praplan, A. P., Pringle, K., Rap, A., Richards,
753 N. A. D., Riipinen, I., Rissanen, M. P., Rondo, L., Sarnela, N., Schobesberger, S., Scott, C. E., Seinfeld,
754 J. H., Sipilä, M., Steiner, G., Stozhkov, Y., Stratmann, F., Tome, A., Virtanen, A., Vogel, A. L., Wagner,
755 A. C., Wagner, P. E., Weingartner, E., Wimmer, D., Winkler, P. M., Ye, P. L., Zhang, X., Hansel, A.,
756 Dommen, J., Donahue, N. M., Worsnop, D. R., Baltensperger, U., Kulmala, M., Carslaw, K. S., and
757 Curtius, J.: Ion-induced nucleation of pure biogenic particles, *Nature*, 533, 521-526,
758 10.1038/nature17953, 2016.

759 Knap, H. C. and Jorgensen, S.: Rapid Hydrogen Shift Reactions in Acyl Peroxy Radicals, *J. Phys. Chem.*
760 *A*, 121, 1470-1479, 10.1021/acs.jpca.6b12787, 2017.

761 Krechmer, J. E., Coggon, M. M., Massoli, P., Nguyen, T. B., Crouse, J. D., Hu, W. W., Day, D. A.,
762 Tyndall, G. S., Henze, D. K., Rivera-Rios, J. C., Nowak, J. B., Kimmel, J. R., Mauldin, R. L., Stark, H.,
763 Jayne, J. T., Sipilä, M., Junninen, H., St Clair, J. M., Zhang, X., Feiner, P. A., Zhang, L., Miller, D. O.,
764 Brune, W. H., Keutsch, F. N., Wennberg, P. O., Seinfeld, J. H., Worsnop, D. R., Jimenez, J. L., and
765 Canagaratna, M. R.: Formation of Low Volatility Organic Compounds and Secondary Organic Aerosol
766 from Isoprene Hydroxyhydroperoxide Low-NO Oxidation, *Environ. Sci. Technol.*, 49, 10330-10339,
767 10.1021/acs.est.5b02031, 2015.

768 Lehtipalo, K., Yan, C., Dada, L., Bianchi, F., Xiao, M., Wagner, R., Stolzenburg, D., Ahonen, L. R.,
769 Amorim, A., Baccarini, A., Bauer, P. S., Baumgartner, B., Bergen, A., Bernhammer, A. K., Breitenlechner,
770 M., Brilke, S., Buchholz, A., Mazon, S. B., Chen, D. X., Chen, X. M., Dias, A., Dommen, J., Draper, D.
771 C., Duplissy, J., Ehn, M., Finkenzeller, H., Fischer, L., Frege, C., Fuchs, C., Garmash, O., Gordon, H.,
772 Hakala, J., He, X. C., Heikkinen, L., Heinritzi, M., Helm, J. C., Hofbauer, V., Hoyle, C. R., Jokinen, T.,
773 Kangasluoma, J., Kerminen, V. M., Kim, C., Kirkby, J., Kontkanen, J., Kürten, A., Lawler, M. J., Mai,
774 H. J., Mathot, S., Mauldin, R. L., Molteni, U., Nichman, L., Nie, W., Nieminen, T., Ojdanic, A., Onnela,
775 A., Passananti, M., Petäjä, T., Piel, F., Pospisilova, V., Quéléver, L. L. J., Rissanen, M. P., Rose, C.,
776 Sarnela, N., Schallhart, S., Schuchmann, S., Sengupta, K., Simon, M., Sipilä, M., Tauber, C., Tomé, A.,
777 Tröstl, J., Väisänen, O., Vogel, A. L., Volkamer, R., Wagner, A. C., Wang, M. Y., Weitz, L., Wimmer, D.,
778 Ye, P. L., Ylisirniö, A., Zha, Q. Z., Carslaw, K. S., Curtius, J., Donahue, N. M., Flagan, R. C., Hansel, A.,

779 Riipinen, I., Virtanen, A., Winkler, P. M., Baltensperger, U., Kulmala, M., and Worsnop, D. R.:
780 Multicomponent new particle formation from sulfuric acid, ammonia, and biogenic vapors, *Science*
781 *Advances*, 4, 10.1126/sciadv.aau5363, 2018.

782 Liu, Y. L., Liu, C., Nie, W., Li, Y. Y., Ge, D. F., Chen, L. D., Zhu, C. J., Wang, L., Zhang, Y. X., Liu, T.
783 Y., Qi, X. M., Wang, J. P., Huang, D. D., Wang, Z., Yan, C., Chi, X. G., and Ding, A. J.: Exploring
784 condensable organic vapors and their co-occurrence with PM_{2.5} and O₃ in winter in Eastern China,
785 *Environmental Science-Atmospheres*, 3, 282-297, 10.1039/d2ea00143h, 2023.

786 Liu, Y. L., Nie, W., Li, Y. Y., Ge, D. F., Liu, C., Xu, Z. N., Chen, L. D., Wang, T. Y., Wang, L., Sun, P.,
787 Qi, X. M., Wang, J. P., Xu, Z., Yuan, J., Yan, C., Zhang, Y. J., Huang, D. D., Wang, Z., Donahue, N. M.,
788 Worsnop, D., Chi, X. G., Ehn, M., and Ding, A. J.: Formation of condensable organic vapors from
789 anthropogenic and biogenic volatile organic compounds (VOCs) is strongly perturbed by NO_x in eastern
790 China, *Atmospheric Chemistry and Physics*, 21, 14789-14814, 10.5194/acp-21-14789-2021, 2021.

791 McFiggans, G., Mentel, T. F., Wildt, J., Pullinen, I., Kang, S., Kleist, E., Schmitt, S., Springer, M.,
792 Tillmann, R., Wu, C., Zhao, D. F., Hallquist, M., Faxon, C., Le Breton, M., Hallquist, A. M., Simpson,
793 D., Bergstrom, R., Jenkin, M. E., Ehn, M., Thornton, J. A., Alfarra, M. R., Bannan, T. J., Percival, C. J.,
794 Priestley, M., Topping, D., and Kiendler-Scharr, A.: Secondary organic aerosol reduced by mixture of
795 atmospheric vapours, *Nature*, 565, 587-593, 10.1038/s41586-018-0871-y, 2019.

796 Meder, M., Graeffe, F., Luo, Y., Luo, J., Iyer, S., Valiev, R., Cai, R., Rissanen, M., Kurtén, T., Varelas, J.
797 G., Geiger, F. M., Thomson, R. J., and Ehn, M.: Selective Deuteration Reveals the Importance of Multiple
798 Branching Pathways in α -Pinene Autoxidation, *J. Am. Chem. Soc.*, 147, 14131-14138,
799 10.1021/jacs.4c14462, 2025.

800 Moller, K. H., Bates, K. H., and Kjaergaard, H. G.: The Importance of Peroxy Radical Hydrogen-Shift
801 Reactions in Atmospheric Isoprene Oxidation, *J. Phys. Chem. A*, 123, 920-932,
802 10.1021/acs.jpca.8b10432, 2019.

803 Moller, K. H., Otkjær, R. V., Hyttinen, N., Kurtén, T., and Kjaergaard, H. G.: Cost-Effective
804 Implementation of Multiconformer Transition State Theory for Peroxy Radical Hydrogen Shift Reactions,
805 *J. Phys. Chem. A*, 120, 10072-10087, 10.1021/acs.jpca.6b09370, 2016.

806 Murphy, S. E., Crouse, J. D., Poulsen, A. S., Lipson, J. E., Kjaergaard, H. G., and Wennberg, P. O.:
807 Accretion product formation in the self- and cross-reactions of small β -hydroxy peroxy radicals, *Environ.*
808 *Sci. - Atmospheres*, 5, 1312-1325, 10.1039/d5ea00106d, 2025.

809 Ng, N. L., Kwan, A. J., Surratt, J. D., Chan, A. W. H., Chhabra, P. S., Sorooshian, A., Pye, H. O. T.,
810 Crouse, J. D., Wennberg, P. O., Flagan, R. C., and Seinfeld, J. H.: Secondary organic aerosol (SOA)
811 formation from reaction of isoprene with nitrate radicals (NO₃), *Atmos. Chem. Phys.*, 8, 4117-4140,
812 10.5194/acp-8-4117-2008, 2008.

813 Nguyen, T. B., Coggon, M. M., Bates, K. H., Zhang, X., Schwantes, R. H., Schilling, K. A., Loza, C. L.,
814 Flagan, R. C., Wennberg, P. O., and Seinfeld, J. H.: Organic aerosol formation from the reactive uptake
815 of isoprene epoxydiols (IEPOX) onto non-acidified inorganic seeds, *Atmospheric Chemistry and Physics*,
816 14, 3497-3510, 10.5194/acp-14-3497-2014, 2014.

817 Nguyen, T. B., Bates, K. H., Crouse, J. D., Schwantes, R. H., Zhang, X., Kjaergaard, H. G., Surratt, J.
818 D., Lin, P., Laskin, A., Seinfeld, J. H., and Wennberg, P. O.: Mechanism of the hydroxyl radical oxidation
819 of methacryloyl peroxyxynitrate (MPAN) and its pathway toward secondary organic aerosol formation in
820 the atmosphere, *Phys. Chem. Chem. Phys.*, 17, 17914-17926, 10.1039/c5cp02001h, 2015.

821 Nie, W., Yan, C., Huang, D. D., Wang, Z., Liu, Y., Qiao, X., Guo, Y., Tian, L., Zheng, P., Xu, Z., Li, Y.,
822 Xu, Z., Qi, X., Sun, P., Wang, J., Zheng, F., Li, X., Yin, R., Dallenbach, K. R., Bianchi, F., Petäjä, T.,

823 Zhang, Y., Wang, M., Schervish, M., Wang, S., Qiao, L., Wang, Q., Zhou, M., Wang, H., Yu, C., Yao, D.,
824 Guo, H., Ye, P., Lee, S., Li, Y. J., Liu, Y., Chi, X., Kerminen, V.-M., Ehn, M., Donahue, N. M., Wang, T.,
825 Huang, C., Kulmala, M., Worsnop, D., Jiang, J., and Ding, A.: Secondary organic aerosol formed by
826 condensing anthropogenic vapours over China's megacities, *Nature Geoscience*, 15, 255-261,
827 [10.1038/s41561-022-00922-5](https://doi.org/10.1038/s41561-022-00922-5), 2022.

828 Nie, W., Yan, C., Yang, L., Roldin, P., Liu, Y., Vogel, A. L., Molteni, U., Stolzenburg, D., Finkenzeller,
829 H., Amorim, A., Bianchi, F., Curtius, J., Dada, L., Draper, D. C., Duplissy, J., Hansel, A., He, X.-C.,
830 Hofbauer, V., Jokinen, T., Kim, C., Lehtipalo, K., Nichman, L., Mauldin, R. L., Makhmutov, V., Mentler,
831 B., Mizelli-Ojdanic, A., Petäjä, T., Quéléver, L. L. J., Schallhart, S., Simon, M., Tauber, C., Tomé, A.,
832 Volkamer, R., Wagner, A. C., Wagner, R., Wang, M., Ye, P., Li, H., Huang, W., Qi, X., Lou, S., Liu, T.,
833 Chi, X., Dommen, J., Baltensperger, U., El Haddad, I., Kirkby, J., Worsnop, D., Kulmala, M., Donahue,
834 N. M., Ehn, M., and Ding, A.: NO at low concentration can enhance the formation of highly oxygenated
835 biogenic molecules in the atmosphere, *Nat. Commun.*, 14, 3347, [10.1038/s41467-023-39066-4](https://doi.org/10.1038/s41467-023-39066-4), 2023.

836 Otkjaer, R. V., Jakobsen, H. H., Tram, C. M., and Kjaergaard, H. G.: Calculated Hydrogen Shift Rate
837 Constants in Substituted Alkyl Peroxy Radicals, *J. Phys. Chem. A*, 122, 8665-8673,
838 [10.1021/acs.jpca.8b06223](https://doi.org/10.1021/acs.jpca.8b06223), 2018.

839 Paulot, F., Crouse, J. D., Kjaergaard, H. G., Kürten, A., St Clair, J. M., Seinfeld, J. H., and Wennberg,
840 P. O.: Unexpected Epoxide Formation in the Gas-Phase Photooxidation of Isoprene, *Science*, 325, 730-
841 733, [10.1126/science.1172910](https://doi.org/10.1126/science.1172910), 2009.

842 Peräkylä, O., Berndt, T., Franzon, L., Hasan, G., Meder, M., Valiev, R. R., Daub, C. D., Varelas, J. G.,
843 Geiger, F. M., Thomson, R. J., Rissanen, M., Kurtén, T., and Ehn, M.: Large Gas-Phase Source of Esters
844 and Other Accretion Products in the Atmosphere, *J. Am. Chem. Soc.*, 145, 7780-7790,
845 [10.1021/jacs.2c10398](https://doi.org/10.1021/jacs.2c10398), 2023.

846 Praske, E., Otkjaer, R. V., Crouse, J. D., Hethcox, J. C., Stoltz, B. M., Kjaergaard, H. G., and Wennberg,
847 P. O.: Atmospheric autoxidation is increasingly important in urban and suburban North America, *Proc.*
848 *Natl. Acad. Sci. U. S. A.*, 115, 64-69, [10.1073/pnas.1715540115](https://doi.org/10.1073/pnas.1715540115), 2018.

849 Riccobono, F., Schobesberger, S., Scott, C. E., Dommen, J., Ortega, I. K., Rondo, L., Almeida, J.,
850 Amorim, A., Bianchi, F., Breitenlechner, M., David, A., Downard, A., Dunne, E. M., Duplissy, J., Ehrhart,
851 S., Flagan, R. C., Franchin, A., Hansel, A., Junninen, H., Kajos, M., Keskinen, H., Kupc, A., Kurten, A.,
852 Kvashin, A. N., Laaksonen, A., Lehtipalo, K., Makhmutov, V., Mathot, S., Nieminen, T., Onnela, A.,
853 Petaja, T., Praplan, A. P., Santos, F. D., Schallhart, S., Seinfeld, J. H., Sipila, M., Spracklen, D. V.,
854 Stozhkov, Y., Stratmann, F., Tome, A., Tsagkogeorgas, G., Vaattovaara, P., Viisanen, Y., Vrtala, A.,
855 Wagner, P. E., Weingartner, E., Wex, H., Wimmer, D., Carslaw, K. S., Curtius, J., Donahue, N. M., Kirkby,
856 J., Kulmala, M., Worsnop, D. R., and Baltensperger, U.: Oxidation Products of Biogenic Emissions
857 Contribute to Nucleation of Atmospheric Particles, *Science*, 344, 717-721, [10.1126/science.1243527](https://doi.org/10.1126/science.1243527),
858 2014.

859 Richters, S., Herrmann, H., and Berndt, T.: Highly Oxidized RO₂ Radicals and Consecutive Products
860 from the Ozonolysis of Three Sesquiterpenes, *Environ. Sci. Technol.*, 50, 2354-2362,
861 [10.1021/acs.est.5b05321](https://doi.org/10.1021/acs.est.5b05321), 2016a.

862 Richters, S., Herrmann, H., and Berndt, T.: Different pathways of the formation of highly oxidized
863 multifunctional organic compounds (HOMs) from the gas-phase ozonolysis of β -caryophyllene,
864 *Atmospheric Chemistry and Physics*, 16, 9831-9845, [10.5194/acp-16-9831-2016](https://doi.org/10.5194/acp-16-9831-2016), 2016b.

865 Riva, M., Rantala, P., Krechmer, J. E., Peräkylä, O., Zhang, Y. J., Heikkinen, L., Garmash, O., Yan, C.,
866 Kulmala, M., Worsnop, D., and Ehn, M.: Evaluating the performance of five different chemical ionization

867 techniques for detecting gaseous oxygenated organic species, *Atmos. Meas. Tech.*, 12, 2403-2421,
868 10.5194/amt-12-2403-2019, 2019.

869 Roldin, P., Eriksson, A. C., Nordin, E. Z., Hermansson, E., Mogensen, D., Rusanen, A., Boy, M.,
870 Swietlicki, E., Svenningsson, B., Zelenyuk, A., and Pagels, J.: Modelling non-equilibrium secondary
871 organic aerosol formation and evaporation with the aerosol dynamics, gas- and particle-phase chemistry
872 kinetic multilayer model ADCHAM, *Atmospheric Chemistry and Physics*, 14, 7953-7993, 10.5194/acp-
873 14-7953-2014, 2014.

874 Roldin, P., Ehn, M., Kurtén, T., Olenius, T., Rissanen, M. P., Sarnela, N., Elm, J., Rantala, P., Hao, L.,
875 Hyttinen, N., Heikkinen, L., Worsnop, D. R., Pichelstorfer, L., Xavier, C., Clusius, P., Öström, E., Petäjä,
876 T., Kulmala, M., Vehkamäki, H., Virtanen, A., Riipinen, I., and Boy, M.: The role of highly oxygenated
877 organic molecules in the Boreal aerosol-cloud-climate system, *Nat. Commun.*, 10, 4370,
878 10.1038/s41467-019-12338-8, 2019.

879 Schervish, M. and Donahue, N. M.: Peroxy radical chemistry and the volatility basis set, *Atmospheric*
880 *Chemistry and Physics*, 20, 1183-1199, 10.5194/acp-20-1183-2020, 2020.

881 Schervish, M., Heinritzi, M., Stolzenburg, D., Dada, L., Wang, M. Y., Ye, Q., Hofbauer, V., Devivo, J.,
882 Bianchi, F., Brilke, S., Duplissy, J., El Haddad, I., Finkenzeller, H., He, X. C., Kuvshinov, A., Kim, C.,
883 Kirkby, J., Kulmala, M., Lehtipalo, K., Lopez, B., Makhmutov, V., Mentler, B., Molteni, U., Nie, W.,
884 Petäjä, T., Quéléver, L., Volkamer, R., Wagner, A. C., Winkler, P., Yan, C., and Donahue, N. M.:
885 Interactions of peroxy radicals from monoterpene and isoprene oxidation simulated in the radical
886 volatility basis set, *Environmental Science-Atmospheres*, 4, 740-753, 10.1039/d4ea00056k, 2024.

887 Shen, H. R., Vereecken, L., Kang, S. A., Pullinen, I., Fuchs, H., Zhao, D. F., and Mentel, T. F.: Unexpected
888 significance of a minor reaction pathway in daytime formation of biogenic highly oxygenated organic
889 compounds, *Science Advances*, 8, 10.1126/sciadv.abp8702, 2022.

890 Shen, J. L., Russell, D. M., Devivo, J., Kunkler, F., Baalbaki, R., Mentler, B., Scholz, W., Yu, W. J.,
891 Caudillo-Plath, L., Sommer, E., Ahongshangbam, E., Alfaouri, D., Almeida, J., Amorim, A., Beck, L. J.,
892 Beckmann, H., Berntheusel, M., Bhattacharyya, N., Canagaratna, M. R., Chassaing, A., Cruz-Simbron,
893 R., Dada, L., Duplissy, J., Gordon, H., Granzin, M., Schute, L. G., Heinritzi, M., Iyer, S., Klebach, H.,
894 Krueger, T., Kuerten, A., Lampimaeki, M., Liu, L., Lopez, B., Martinez, M., Morawiec, A., Onnela, A.,
895 Peltola, M., Rato, P., Reza, M., Richter, S., Roerup, B., Sebastian, M. K., Simon, M., Surdu, M., Tamme,
896 K., Thakur, R. C., Tome, A., Tong, Y. D., Top, J., Umo, N. S., Unfer, G., Vettikkat, L., Weissbacher, J.,
897 Xenofontos, C., Yang, B. X., Zauner-Wieczorek, M., Zhang, J. Y., Zheng, Z. S., Baltensperger, U.,
898 Christoudias, T., Flagan, R. C., El Haddad, I., Junninen, H., Moehler, O., Riipinen, I., Rohner, U.,
899 Schobesberger, S., Volkamer, R., Winkler, P. M., Hansel, A., Lehtipalo, K., Donahue, N. M., Lelieveld,
900 J., Harder, H., Kulmala, M., Worsnop, D. R., Kirkby, J., Curtius, J., and He, X. C.: New particle formation
901 from isoprene under upper-tropospheric conditions, *Nature*, 636, 10.1038/s41586-024-08196-0, 2024.

902 Simon, M., Dada, L., Heinritzi, M., Scholz, W., Stolzenburg, D., Fischer, L., Wagner, A. C., Kurten, A.,
903 Rorup, B., He, X. C., Almeida, J., Baalbaki, R., Baccarini, A., Bauer, P. S., Beck, L., Bergen, A., Bianchi,
904 F., Brakling, S., Brilke, S., Caudillo, L., Chen, D. X., Chu, B. W., Dias, A., Draper, D. C., Duplissy, J.,
905 El-Haddad, I., Finkenzeller, H., Frege, C., Gonzalez-Carracedo, L., Gordon, H., Granzin, M., Hakala, J.,
906 Hofbauer, V., Hoyle, C. R., Kim, C., Kong, W. M., Lamkaddam, H., Lee, C. P., Lehtipalo, K., Leiminger,
907 M., Mai, H. J., Manninen, H. E., Marie, G., Marten, R., Mentler, B., Molteni, U., Nichman, L., Nie, W.,
908 Ojdanic, A., Onnela, A., Partoll, E., Petaja, T., Pfeifer, J., Philippov, M., Quelever, L. L. J., Ranjithkumar,
909 A., Rissanen, M. P., Schallhart, S., Schobesberger, S., Schuchmann, S., Shen, J. L., Sipila, M., Steiner,
910 G., Stozhkov, Y., Tauber, C., Tham, Y. J., Tome, A. R., Vazquez-Pufleau, M., Vogel, A. L., Wagner, R.,

911 Wang, M. Y., Wang, D. S., Wang, Y. H., Weber, S. K., Wu, Y. S., Xiao, M., Yan, C., Ye, P. L., Ye, Q.,
912 Zauner-Wieczorek, M., Zhou, X. Q., Baltensperger, U., Dommen, J., Flagan, R. C., Hansel, A., Kulmala,
913 M., Volkamer, R., Winkler, P. M., Worsnop, D. R., Donahue, N. M., Kirkby, J., and Curtius, J.: Molecular
914 understanding of new-particle formation from alpha-pinene between -50 and +25 °C, *Atmospheric*
915 *Chemistry and Physics*, 20, 9183-9207, 10.5194/acp-20-9183-2020, 2020.

916 Sindelarova, K., Granier, C., Bouarar, I., Guenther, A., Tilmes, S., Stavrou, T., Müller, J. F., Kuhn, U.,
917 Stefani, P., and Knorr, W.: Global data set of biogenic VOC emissions calculated by the MEGAN model
918 over the last 30 years, *Atmospheric Chemistry and Physics*, 14, 9317-9341, 10.5194/acp-14-9317-2014,
919 2014.

920 Stolzenburg, D., Fischer, L., Vogel, A. L., Heinritzi, M., Schervish, M., Simon, M., Wagner, A. C., Dada,
921 L., Ahonen, L. R., Amorim, A., Baccarini, A., Bauer, P. S., Baumgartner, B., Bergen, A., Bianchi, F.,
922 Breitenlechner, M., Brilke, S., Mazon, S. B., Chen, D. X., Dias, A., Draper, D. C., Duplissy, J., Haddad,
923 I., Finkenzeller, H., Frege, C., Fuchs, C., Garmash, O., Gordon, H., He, X., Helm, J., Hofbauer, V., Hoyle,
924 C. R., Kim, C., Kirkby, J., Kontkanen, J., Kuerten, A., Lampilahti, J., Lawler, M., Lehtipalo, K.,
925 Leiminger, M., Mai, H., Mathot, S., Mentler, B., Molteni, U., Nie, W., Nieminen, T., Nowak, J. B.,
926 Ojdanic, A., Onnela, A., Passananti, M., Petaja, T., Quelever, L. L. J., Rissanen, M. P., Sarnela, N.,
927 Schallhart, S., Tauber, C., Tome, A., Wagner, R., Wang, M., Weitz, L., Wimmer, D., Xiao, M., Yan, C.,
928 Ye, P., Zha, Q., Baltensperger, U., Curtius, J., Dommen, J., Flagan, R. C., Kulmala, M., Smith, J. N.,
929 Worsnop, D. R., Hansel, A., Donahue, N. M., and Winkler, P. M.: Rapid growth of organic aerosol
930 nanoparticles over a wide tropospheric temperature range, *Proc. Natl. Acad. Sci. U. S. A.*, 115, 9122-
931 9127, 10.1073/pnas.1807604115, 2018.

932 Trostl, J., Chuang, W. K., Gordon, H., Heinritzi, M., Yan, C., Molteni, U., Ahlm, L., Frege, C., Bianchi,
933 F., Wagner, R., Simon, M., Lehtipalo, K., Williamson, C., Craven, J. S., Duplissy, J., Adamov, A.,
934 Almeida, J., Bernhammer, A. K., Breitenlechner, M., Brilke, S., Dias, A., Ehrhart, S., Flagan, R. C.,
935 Franchin, A., Fuchs, C., Guida, R., Gysel, M., Hansel, A., Hoyle, C. R., Jokinen, T., Junninen, H.,
936 Kangasluoma, J., Keskinen, H., Kim, J., Krapf, M., Kurten, A., Laaksonen, A., Lawler, M., Leiminger,
937 M., Mathot, S., Mohler, O., Nieminen, T., Onnela, A., Petaja, T., Piel, F. M., Miettinen, P., Rissanen, M.
938 P., Rondo, L., Sarnela, N., Schobesberger, S., Sengupta, K., Sipila, M., Smith, J. N., Steiner, G., Tome,
939 A., Virtanen, A., Wagner, A. C., Weingartner, E., Wimmer, D., Winkler, P. M., Ye, P. L., Carslaw, K. S.,
940 Curtius, J., Dommen, J., Kirkby, J., Kulmala, M., Riipinen, I., Worsnop, D. R., Donahue, N. M., and
941 Baltensperger, U.: The role of low-volatility organic compounds in initial particle growth in the
942 atmosphere, *Nature*, 533, 527-531, 10.1038/nature18271, 2016.

943 Wang, S. N., Riva, M., Yan, C., Ehn, M., and Wang, L. M.: Primary Formation of Highly Oxidized
944 Multifunctional Products in the OH-Initiated Oxidation of Isoprene: A Combined Theoretical and
945 Experimental Study, *Environ. Sci. Technol.*, 52, 12255-12264, 10.1021/acs.est.8b02783, 2018.

946 Weber, J., Archer-Nicholls, S., Griffiths, P., Berndt, T., Jenkin, M., Gordon, H., Knote, C., and Archibald,
947 A. T.: CRI-HOM: A novel chemical mechanism for simulating highly oxygenated organic molecules
948 (HOMs) in global chemistry-aerosol-climate models, *Atmospheric Chemistry and Physics*, 20, 10889-
949 10910, 10.5194/acp-20-10889-2020, 2020.

950 Wennberg, P. O., Bates, K. H., Crouse, J. D., Dodson, L. G., McVay, R. C., Mertens, L. A., Nguyen, T.
951 B., Praske, E., Schwantes, R. H., Smarte, M. D., St Clair, J. M., Teng, A. P., Zhang, X., and Seinfeld, J.
952 H.: Gas-Phase Reactions of Isoprene and Its Major Oxidation Products, *Chem. Rev.*, 118, 3337-3390,
953 10.1021/acs.chemrev.7b00439, 2018.

954 Xu, Z. N., Nie, W., Liu, Y. L., Sun, P., Huang, D. D., Yan, C., Krechmer, J., Ye, P. L., Xu, Z., Qi, X. M.,

955 Zhu, C. J., Li, Y. Y., Wang, T. Y., Wang, L., Huang, X., Tang, R. Z., Guo, S., Xiu, G. L., Fu, Q. Y.,
956 Worsnop, D., Chi, X. G., and Ding, A. J.: Multifunctional Products of Isoprene Oxidation in Polluted
957 Atmosphere and Their Contribution to SOA, *Geophysical Research Letters*, 48, 10.1029/2020gl089276,
958 2021.

959 Yang, H., Raucci, U., Iyer, S., Hasan, G., Almeida, T. G., Barua, S., Savolainen, A., Kangasluoma, J.,
960 Rissanen, M., Vehkamäki, H., and Kurtén, T.: Molecular dynamics-guided reaction discovery reveals
961 endoperoxide-to-alkoxy radical isomerization as key branching point in α -pinene ozonolysis, *Nat.*
962 *Commun.*, 16, 12, 10.1038/s41467-025-55985-w, 2025.

963 [Yang, L., Roldin, P., and Nie, W.: SIM-HOM model \(version 1.0\). Zenodo.](https://doi.org/10.5281/zenodo.19047874)
964 <https://doi.org/10.5281/zenodo.19047874>, 2026.

965 Zha, Q. Z., Aliaga, D., Krejci, R., Sinclair, V. A., Wu, C., Ciarelli, G., Scholz, W., Heikkinen, L., Partoll,
966 E., Gramlich, Y., Huang, W., Leiminger, M., Enroth, J., Peräkylä, O., Cai, R. L., Chen, X. M., Koenig,
967 A. M., Velarde, F., Moreno, I., Petäjä, T., Artaxo, P., Laj, P., Hansel, A., Carbone, S., Kulmala, M.,
968 Andrade, M., Worsnop, D., Mohr, C., and Bianchi, F.: Oxidized organic molecules in the tropical free
969 troposphere over Amazonia, *Natl. Sci. Rev.*, 11, 11, 10.1093/nsr/nwad138, 2024.

970 Zhao, D. F., Pullinen, I., Fuchs, H., Schrade, S., Wu, R. R., Acir, I. H., Tillmann, R., Rohrer, F., Wildt, J.,
971 Guo, Y. D., Kiendler-Scharr, A., Wahner, A., Kang, S., Vereecken, L., and Mentel, T. F.: Highly
972 oxygenated organic molecule (HOM) formation in the isoprene oxidation by NO₃ radical, *Atmospheric*
973 *Chemistry and Physics*, 21, 9681-9704, 10.5194/acp-21-9681-2021, 2021.

974